# THE SAMARA SPACECRAFT: DESIGN AND DEVELOPMENT OF A SELF-STABILIZING, AUTO-ROTATING, DISTRIBUTED SENSING SYSTEM

by

AMIT DESAI LALLOOBHAI

Presented to the Faculty of the Graduate School of

The University of Texas at Arlington in Partial Fulfillment

of the Requirements

for the Degree of

MASTER OF SCIENCE IN AEROSPACE ENGINEERING

THE UNIVERSITY OF TEXAS AT ARLINGTON

May 2013

ACKNOWLEDGEMENTS

I would like to thank Ben Harris for his role as my advisor and mentor throughout my graduate career. His support and guidance helped turn my ideas into a reality. I would like the thank Mousumi Ahmed, Ziad Bakhaya, and Tracie Perez for their continued support throughout this research project. I would like to acknowledge the entire Satellite Technology Laboratory for being a wonderful group of colleagues whom I enjoyed the company of the past two years.

I would like to thank my wife, Kinjal, for being the best partner in life. Thank you for believing in me and giving me the strength to believe in myself. I would like to thank my Mother for brightening every day of my life. I also want to thank my grandparents, uncles and aunts, brothers, sisters, cousins, and my nephew and niece for your love, support, and motivation throughout my life. I am proud to say you all have molded me into the person I am today. Thank you to Devanshu for being my best friend.

Finally, I would like to thank my Father, whom I dedicate this thesis to. Thank you for always pushing me to better myself. You pushed me towards countless opportunities and taught me the meaning of hard work.

April 22, 2013

ABSTRACT

THE SAMARA SPACECRAFT: DESIGN AND DEVELOPMENT OF A SELF-STABILIZING, AUTO-ROTATING, DISTRIBUTED SENSING SYSTEM

Amit D. Lalloobhai, M.S. Aerospace Engineering
The University of Texas at Arlington, 2013

Supervising Professor: Ben Harris

The scope of this research is the design and development of a self-stabilizing re-entry vehicle that closely resembles naturally occurring seeds in nature. It was hypothesized that a femto-satellite with a shape of a samara could self stabilize and passively generate lift, as well as transmit a signal during its descent through the atmosphere. The research included a conceptual design phase and a preliminary design phase that entailed analytic simulations, and an experimental demonstration. The goal was to investigate the feasibility of developing the above-mentioned femto-vehicle that could increase the range capability of its descent to maximize data capture.

TABLE OF CONTENTS

LIST OF FIGURES

Figure Page

LIST OF TABLES

# NOMENCLATURE

| | |
|---|---|
| A | aerodynamic force parallel to blade element section |
| C | direction cosine matrix |
| $C_d$ | blade element coefficient of drag |
| $C_l$ | blade element coefficient of lift |
| $C_R$ | centrifugal force acting near samara root |
| $C_T$ | centrifugal force acting near samara tip |
| $C_x$, $C_y$, $C_z$ | distances specifying center of mass location |
| D | drag |
| F | external force |
| H | angular momentum |
| I | mass moment of inertia |
| L | lift |
| M | external moment vector ($M_x$; $M_y$; $M_z$) |
| N | aerodynamic force perpendicular to blade element section |
| P | linear momentum |
| $P_{cr}$ | Moment arm that $C_R$ acts through |
| $P_{ct}$ | Moment arm that $C_T$ acts through |
| R | position vector ($R_1$; $R_2$; $R_3$) |
| $R_l$ | length of samara blade |
| S | matrix specific to 3-2-1 rotation sequence to relate angular velocity components to Euler time derivatives |
| T | Thrust of a rotor |
| U | resultant air velocity experienced by blade element |
| $U_P$ | resultant air velocity perpendicular to rotor plane |
| $U_T$ | resultant air velocity tangential to blade element |
| V | velocity vector ($v_1$; $v_2$; $v_3$) |
| $V_v$ | air velocity due to vehicle's descent rate |

| | |
|---|---|
| W | weight |
| **X** | state vector $[\omega;\ \Theta;\ V;\ R]$ |
| X, Y, Z | body frame coordinates used for Blade Element Momentum Theory analysis |
| a | section lift curve slope |
| b | number of blades |
| $\widehat{b_1}, \widehat{b_2}, \widehat{b_3}$ | body frame unit-vectors |
| c | blade element chord |
| $\widehat{\imath_1}, \widehat{\imath_2}, \widehat{\imath_3}$ | inertial frame unit-vectors |
| $m$ | mass |
| r | radial distance from root to blade element |
| $r_{cp}$ | spanwise distance from center of mass to center of pressure |
| $r_{cr}$ | horizontal distance from center of mass to point of action of $C_R$ |
| $r_{ct}$ | horizontal distance from center of mass to point of action of $C_T$ |
| y | non-dimensional radial distance from root to blade element |
| $\Theta$ | orientation vector $[\phi;\ \theta;\ \psi]$ |
| $\alpha$ | angle of attack |
| $\phi, \theta, \psi$ | Euler angles (roll, pitch, yaw) |
| $\rho$ | air density |
| $v_i$ | rotor induced velocity |
| $\omega$ | angular velocity vector $[\omega_1;\ \omega_2;\ \omega_3]$ |

# CHAPTER 1

# INTRODUCTION

The objective of this research is the design and development of a self-stabilizing re-entry vehicle that closely resembles naturally occurring seeds in nature. It is hypothesized that a femto-satellite vehicle with a shape of a samara could self stabilize and passively generate lift, as well as transmit a signal during its descent through the atmosphere. This research includes a conceptual design phase and a preliminary design phase that entails analytic simulations, and an experimental demonstration. The goal is to investigate the feasibility of developing the above-mentioned femto- vehicle that could increase the range capability of its descent to maximize data capture in a distributed sensor mission.

Figure 1.1: Prototype samara vehicle with Inertial Measurement Sensor payload

## 1.1 Small Satellites

The availability of commercial off-the-shelf (COTS) hardware and software have allowed for a new breed of satellite missions and satellites to form. Missions can become more reliable with affordable redundant systems available to backup

critical elements of the mission operations. As the industry capability on electronic packaging becomes increasingly optimized, complete satellite systems are able to fit in smaller and smaller volumes, dramatically reducing the mass budget and overall mission cost. Pico-satellites, or 1-kilogram satellites, have become easily accessible to a wide range of platforms, including research, academia, and industry. There are even startup companies, such as Skybox Imaging, who are developing high performance constellations of imaging satellites to deliver high-resolution images to their clients.

Femto-satellites are an even smaller class of satellites on the order of 10-100 grams, and have only recently been investigated in detail. Because of advancements in the field of nanotechnology, in particular electronic packaging, a system that requires several integrated sub-systems could fit on a single chip. Multichip module technology is a specialized electronic package where multiple discrete components are packaged onto a single substrate, enabling their use as a single integrated circuit. In an effort to understand and fabricate a system-on-a-chip (SoC), projects such as the Smart Dust project are investigating methods for creating autonomous wireless sensor nodes, which incorporate sensing, power, computation, and communication into one system [1]. With this growing trend in utilizing very small satellites working within a system, it is possible to recognize and implement space missions that were previously considered not possible.

## 1.2 Distributed Space Missions

A distributed satellite system is a system of multiple satellites with a cooperative infrastructure for science measurement, data acquisition, processing,

analysis, and distribution [2]. This definition can be further broken down into two subtypes of distributed satellite missions. The first type is a system that implements multiple satellites in a traditional constellation to meet mission requirements. Constellations do not typically require precise orientation between satellites, but may require a form of station keeping. Satellites in a constellation are linked via ground station systems, and typically do not implement inter-satellite links.

The second type of distributed satellite system establishes the concept of a local cluster with optional formation capabilities, in which "satellites are, by design, placed close together in the same orbit and are fixed on a common target." [3] Formation capabilities would require further complexities because of the exact spacing requirements between the satellites and the level of precision that is defined by the initial project and mission requirements. However, motivation for implementing formation flying of a cluster would allow for generation of virtual apertures, antennas, or other sensors much larger than any individual satellite could achieve.

### 1.2.1 Current Distributed Space Missions

There are numerous examples of distributed satellite systems currently in operation. One in particular is the first and largest distributed communication system, the Iridium global mobile telephone network, which implements 66 LEO communication satellites in a constellation. Iridium is also the only commercial constellation that utilizes inter-satellite links, or crosslinks, which allows satellites in the constellation to communicate directly to other satellites in the system. There are currently two distributed navigation systems, the Global Positioning System

(GPS) pictured in Figure 1.2, and the Russian equivalent, Global Navigation Satellite System (GLONASS).

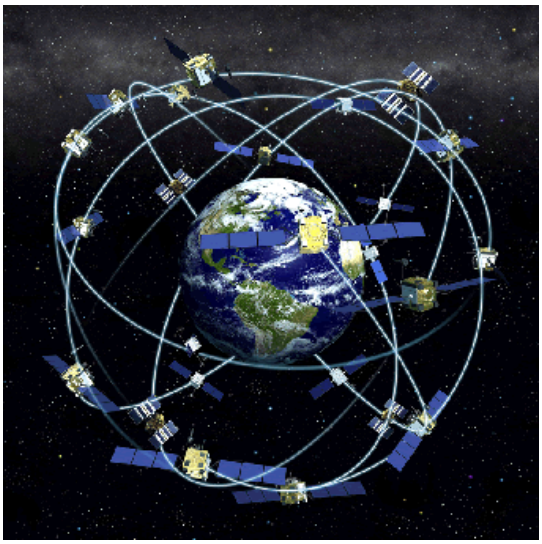

Figure 1.2: GPS constellation, *image courtesy of NIST*

The European Space Agency is also planning on launching their navigation system Galileo in the near future. Current distributed space missions also employ complex orbit designs. Typically, satellite constellations are designed in such a way that each satellite experiences similar perturbations. This allows minimal station keeping requirements. Constellations are also designed with phasing of the satellites within the constellation to avoid collisions and interference. For example, GPS uses 32 satellites placed in six semi-synchronous orbital planes. The orbits are arranged such that at least six satellites are within line of site of almost anywhere on the Earth's surface to deliver accurate position and time data.

### 1.2.2 Potential Distributed Space Missions

With missions such as GPS, GLONASS, and Iridium employing highly successful distributed satellites systems, distributed space missions with increased

requirements and complexities are becoming realized. For example, Stellar Imager, a mission being carried out by NASA Goddard Spaceflight Research Center is an imaging constellation that utilizes aperture synthesizing for extremely high resolution. Stellar Imager will employ 20-30 satellites in a parabolic configuration to act as mirrors and a central hub with focal plane instrumentation.

There is an unrealized class of atmospheric, space weather, and deep space missions for simultaneous measurements of phenomena over a large volume. One interesting mission is the detection, mapping, and study of ionospheric plasma depletions, otherwise known as plasma bubbles [4]. This phenomenon is believed to cause communication and navigation satellite signal outages by scintillating the signal. The understanding gained by such missions would positively impact private, commercial and government sectors. These entities depend on satellite communication and navigation for commerce and political stability as well as military operations. Another proposed mission would be to map the levels of methane on Mars throughout its atmosphere in an effort to determine the source of its creation [5]. Because of its short photochemical lifetime of about 300 years, the existence of methane on Mars indicates recent release from sub-surface reservoirs into the atmosphere. This mission would aid in answering a fundamental question about the existence of life on Mars.

### 1.3 Reference Mission

The reference mission for this research project is an upper atmosphere weather observation experiment. Although this mission is not a true space mission, it serves as testbed to validate the individual capabilities of distributed space

missions being researched. Currently, upper atmosphere observation is conducted using a radiosonde. A radiosonde is an expendable instrument package suspended from a weather balloon and is used for observing the upper atmosphere. The device is capable of sensing pressure, temperature and relative humidity, and sending the sensor measurements via a battery-powered transmitter to a ground station. By tracking the position of the radiosonde in flight, it is possible to obtain information on wind speeds and direction aloft.

In an effort to dramatically increase the spatial diversity of a single radiosonde experiment, this research produced a distributed sensing system that can be released from a single weather balloon. The proposed distributed sensing system would utilize a large number of very small devices each with capabilities matching a single radiosonde, which are then released from a weather balloon launch system at a specified altitude, as shown in Figure 1.3. These individual sensors would descend through the atmosphere while measuring, transmitting, and emitting a tracking signal.

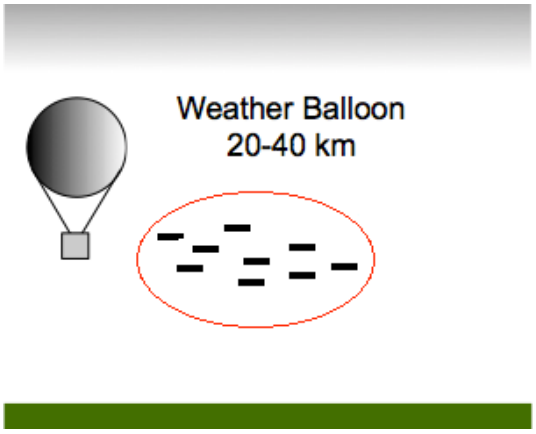


Figure 1.3: Distributed Radiosonde Mission swarm released from weather balloon launch vehicle

## 1.4 Conceptual Design

A clear definition of the gross vehicle design space must be established. This design space is governed by current industry capability, meaning the current technologies readily available for use, and the size and scale of vehicle that can meet the necessary requirements. In order for the missions mentioned above to be successful, it would require a system that would utilize hundreds to thousands of spacecraft in a non-maintained constellation for real-time, multi-point remote sensing with the optional availability crosslink.

### 1.4.1 Parametric Sizing

The parametric sizing of the conceptual design phase involves defining the key parameters that govern the design space possible to accomplish the mission. The following high-level parameters characterize a distributed sensing mission for observing the upper atmosphere. These parameters were adapted from how current radiosonde missions are conducted:

- Define the number of sensing devices to monitor the weather environment in the upper atmosphere.
- Define the instrument suite needed to measure the meteorological parameters and the major subsystems of the vehicle architecture.
- Define the mission operation including launch configuration, flight operations, and data return strategy
- Consider the reliability and affordability of the mission

A feasible way to achieve these design parameters, as well as the parameters defining other distributed space missions, is to scale down the size of the vehicle to

a sub-kilogram level that is mass producible and utilize COTS hardware and software to dramatically reduce the cost of the system. In order to characterize the weather environment of the upper atmosphere, the proposed mission will expose the flight vehicle and science payload to a desired altitude range. The payload suite will contain instruments capable of measuring pressure, temperature, and humidity. The sensor payloads will be sufficiently small enough to fit on a single printed circuit board (PCB) configuration. The parameters do not specify any necessary flight operations; however, maximizing the exposure time of the payload suite would facilitate the increase in spatial resolution capability. Furthermore, maintaining a stable vehicle orientation would satisfy any pointing requirements of the payload suite as well as provide a reliable communication network.

### 1.4.2 Configuration Layout - Femto-satellite

The mission requirements are the main driving force behind the configurations that can be realized. The femto-satellite architecture offers a reasonable and cost effective way of fulfilling the requirements for a distributed radiosonde mission. Figure 1.4 shows examples of reduced-size integrated systems with space application.

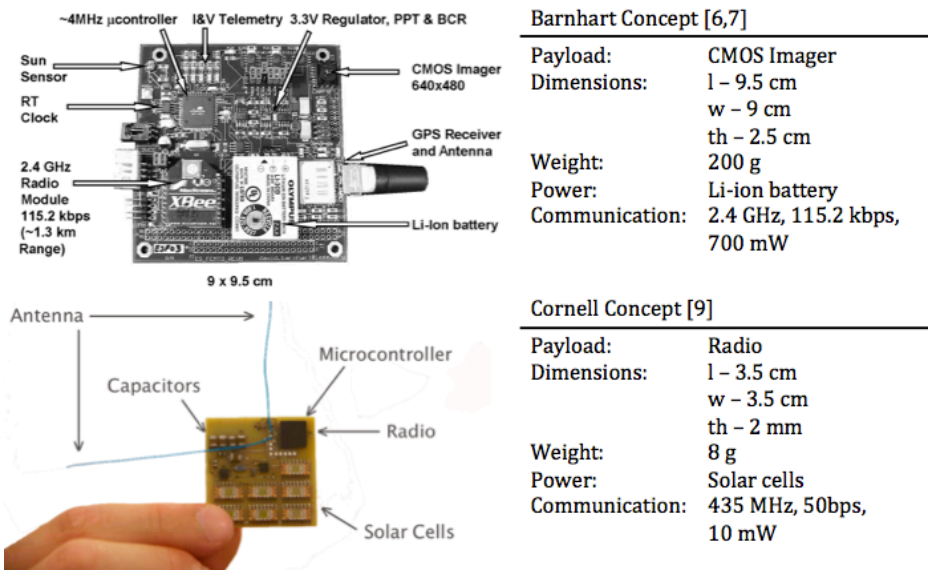


Figure 1.4: Examples of reduced-size integrated systems with space application

Barnhart et al. demonstrated a version of the satellite on a chip that satisfied all the major systems of a typical satellite with a payload. His satellite concept was a system printed on a circuit board with 9 cm x 9.5 cm x 2.5 cm dimensions and an estimated mass of 200 g. The payload was a CMOS imager and served as a proof of concept science payload. With compatibility with existing deployment mechanisms, this system has shown to be a technically viable and cost-effective solution for distributed science missions [6,7,8].

Atchison and Peck developed a single wafer PCB design with solar power. This complete satellite-on-a-chip promises the capability of transmitting a signal from orbit, allowing a ground station to track its position. Because of their extremely small size, these satellites can be packaged and then launched from a parent pico-satellite [9].

A proposed prototype vehicle based on a femto-satellite, or the satellite-on-a-chip design is being investigated. A form factor with a maximum payload weight of 10

grams was chosen.

## 1.5 Design Trades

The chosen configuration offers advantages not possible with traditional satellite designs. However, these advantages do not come without limitation. A satellite design based on a femto-satellite requires a very small form factor to maintain a low mass, thus a low volume. The overall length scale of a femto-satellite is small compared to traditional satellites is small because of the mass constraints. Because of this, a femto-satellite cannot accommodate a traditional propulsion system for trajectory maneuvers or corrections. Extremely small bodies in space can also experience qualitatively different orbits than larger bodies, such that Keplerian orbital mechanics fails to accurately describe the motion. Interplanetary dust can be ejected from our solar system by solar radiation pressure and other electromagnetic forces, and can even be aerocaptured onto Earth's surface without the hypersonic ablation experienced by large meteors [10,11]. S

To mitigate the lack of a traditional propulsion system, unique design approach by Atchison and Peck suggests that very small spacecraft still achieve orbital maneuvers passively. If the characteristic length is sufficiently small enough, the spacecraft can maneuver without the use of propellants by exploiting non-gravitational accelerations such as solar radiation pressure [9,12,13]. The small characteristic length also suggests that an extremely small body can efficiently aerobrake and aerocapture in the presence of an atmosphere, while the effects from aerothermal and radiative heat transfer remain relatively low [10,11,13]. This makes it possible for a small spacecraft to transmit data during a reentry process,

thus making near space observation possible. Near space refers to the region of space higher than weather balloons can reach and lower than the minimum low earth orbit for traditional satellites.

This research extends the reentry architecture of a very small satellite by using the simple geometry of a samara, shown in Figure 1.5, to minimize the descent rate during reentry in the presence of an atmosphere and significantly increase the exposure time to the atmosphere as well as improve the downrange capability of a potential sensing device.

Figure 1.5: Maple seed samara

A samara is a general term that refers to the types of fruits that develop a flattened wing structure over a single seed [14,15]. The biological function of the samara is to decrease its descent rate as it falls to the surface. This increases the horizontal distance, or down range capability, of the seed, aiding in the dispersal potential of the plant. There are two geometries of samaras being investigated for the purpose of this research. The first type of samara has geometry such that the seed is on one side, with the wing extending to the other side, which results in a stable autorotation as the seed falls. The other geometry being considered takes the form of a flying wing body, which experiences gliding flight as it descends. Both of

these geometries are able to achieve steady state stability as they descend as well.

## 1.6 Samara-like Vehicles

Several samara-like vehicles have been developed in the past. The following vehicles take the form of a single-wing samara.

### 1.6.1 Samara-Wing Decelerator

The most developed and documented of these vehicles is the Samara-Wing Decelerator, created by Textron Defense Systems and the US Army Armament Research and Development Center. This system is comprised of a cylindrical payload compartment with an attached rectangular piece of fabric. The fabric "wing" is formed into an aerodynamic surface by the centrifugal load imparted on a weight at its tip. This vehicle must be launched with an initial spin in order to tension the fabric wing, and once spinning causes a passive lunar rotation and steady descent of its payload. Peter Crimi presented a study outlining the development of a seven degree-of-freedom analytical model of this system [16,17]. The decelerator has been employed by Textron as the airframe for several munitions systems. The Selectively Targeted Skeet (STS) submunition is an air launched Samara-Wing Decelerator that houses a shaped charge within its payload canister. Figure 1.6 shows the STS with its cloth wing deployed. A sensor scans the footprint in a tightening spiral. When a target is detected, the shaped charge is fired. Textron has produced several variants of this system, but all use the same fundamental design, and more notably, all are passive systems that lack any control once deployed.

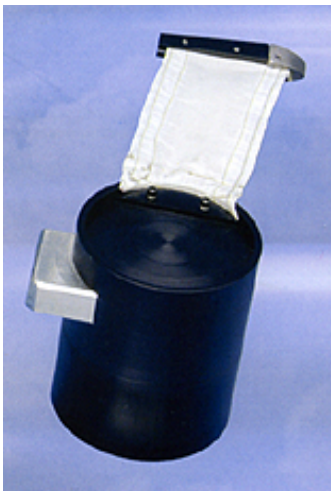

Figure 1.6: Textron selectively targeted Skeet Submunition, *Image courtesy of Textron*

### 1.6.2 Lockheed Martin Samarai

Lockheed Martin has developed a hand-held nano air vehicle called the samarai, shown in Figure 1.7. The samarai is an actively controlled rotating vehicle that demonstrated vertical takeoff and landing, stable hover, and on-board video streaming. The samarai design is also mechanically simple with only two moving parts. In an effort to eliminate expensive production costs and the ability to customize designs to specific mission needs, the samarai was manufactured using a 3-D printer by "printing" successive small layers of plastic to create a single form.

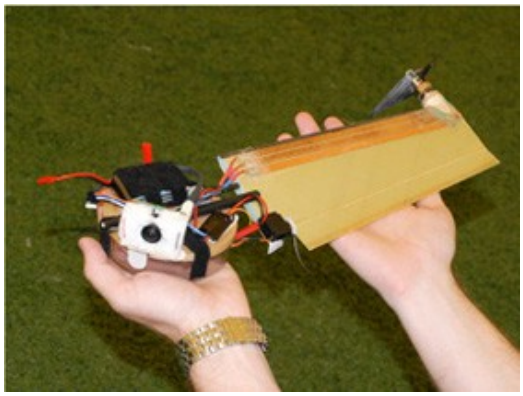

Figure 1.7: Lockheed Martin Samarai, *Image courtesy of Lockheed Martin*

## 1.7 Proposed Vehicle

Consisting of a single wing shape, the samara craft being developed experiences a steady state auto gyration motion as it descends. It is also able to achieve this motion regardless of its initial state and conditions. A slower descent rate allows for an increase in the down range capability during the descent of the vehicle. In an effort to characterize this behavior, a computational simulation was developed to better understand the flight performance of the samara vehicle. This simulation was used to calculate and predict the descent rate and spin rate of the vehicle after it entered a steady state auto-gyration motion.

The nominal samara craft has the capability to start its mission from a low earth orbit, make several orbits, and then transition into a reentry phase where it descends through the atmosphere. The craft will then transition from a hypersonic speed regime to subsonic speeds where the samara shape plays a significant role in the descent rate. The operational view in Figure 1.8 provides a detailed overview of the samara craft's flight operations as well as potential missions the vehicle is suited to accomplish. Currently, some of these altitudes where operation could be achieved by the samara craft, in particular regions encompassing aurora formation and the Meso-pause, cannot be actively investigated.

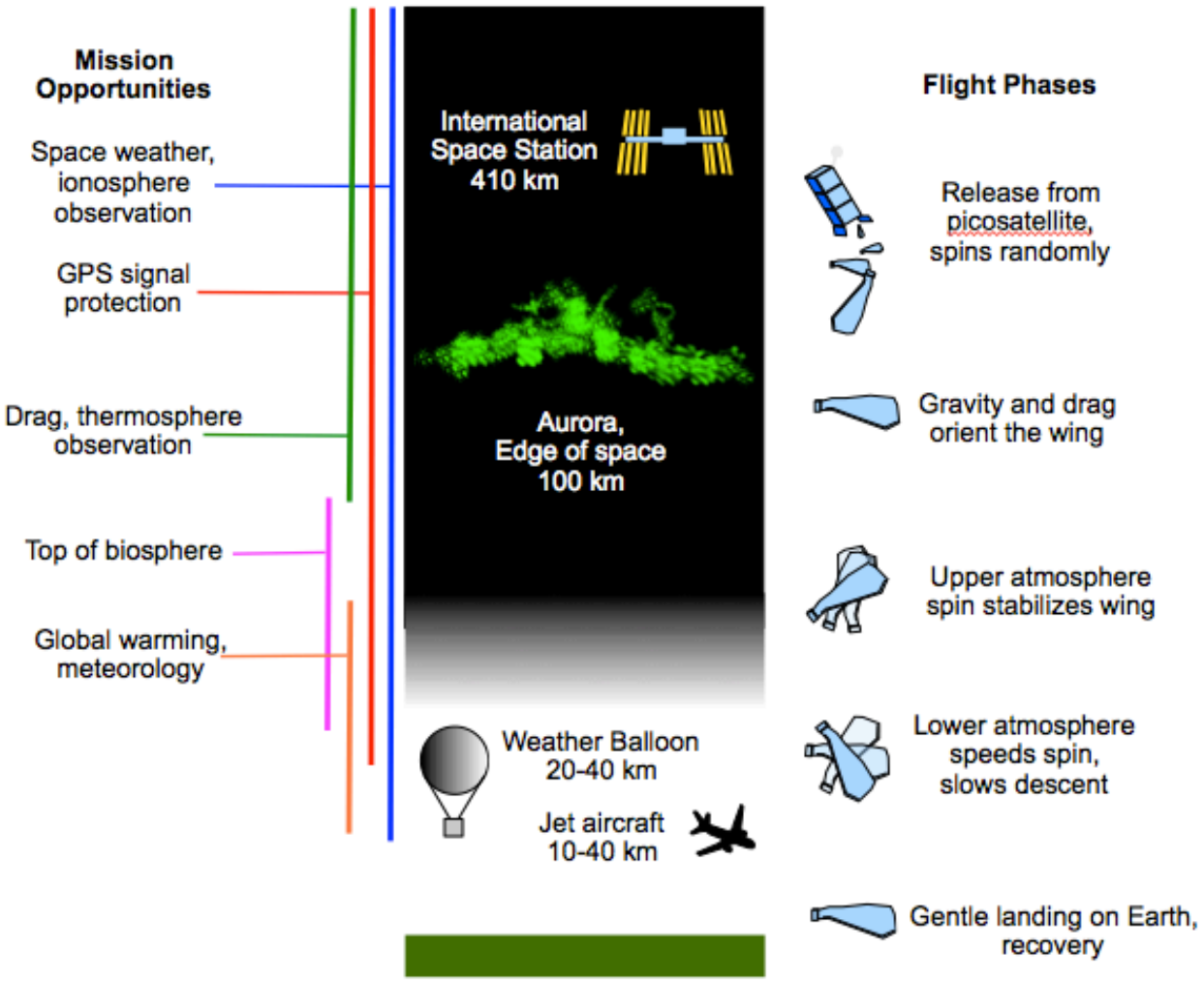


Figure 1.8: Operational View of a distributed sensing system with samara-shaped crafts

## 1.8 Achievements of this Research

Distributed sensing missions are a novel concept and using the geometry of a samara to design a vehicle has only been briefly investigated. Through the design and development of a samara craft, several research discoveries about the stability characteristics of samara flight were made. This research achieved the following milestones:

- Conceptual Design
- Science Investigation for an upper atmosphere mission
- Conceptual mission design for an upper atmosphere mission
- Development of a 6 degree-of-freedom analytical model describing the steady state auto-rotating descent of a samara
- Development of a time simulation to numerically solve the analytical model
- Design of prototype samara models
- Field experiments to validate the simulation
- Flight test of IMU sensing samara

## 1.9 Thesis Outline

This thesis consists of five chapters. Chapter 1 offers a description of the goals of this research, as well as the background studies of small satellite design, distributed space missions, and samara flight behavior. This chapter also introduces the reference distributed mission and samara-shaped sensing device concept. Chapter 2 discusses the mission design and science investigation undertaken to accomplish reference mission, and design attributes of the vehicle. Chapter 3 presents the theory behind the flight behavior of samaras. This chapter also

presents the development of a rigid body dynamic and aerodynamic model to describe this behavior. A simulation was developed to numerically solve the model to predict flight behavior. Chapter 4 details the flight-testing of prototype samara vehicles and the analysis of the results of these tests. Chapter 5 presents a discussion of the work done and lessons learned. Finally, Chapter 6 presents a conclusions as well as the future work needed to advance the concept.

# CHAPTER 2

# MISSION DESIGN AND VEHICLE CONCEPT DEVELOPMENT

This chapter presents the overall nominal mission design and concept development undertaken during the design of the samara craft and the mission it would fly. This development phase included devising systems capable of operating on a very small vehicle in a steady state autorotation flight. This chapter also presents an investigation into the stable flight characteristics of the vehicle geometries being considered.

## 2.1 Mission Design

The nominal samara satellite mission encompasses a system of sensors beginning their operations from LEO and continuously operating through reentry before landing gently on the ground. This mission design refers to the reference mission of a distributed radiosonde mission discussed in Chapter 1, and only considers operation in the upper atmosphere. The mission design includes the science investigation undertaken for the reference mission as well as the mission phases that would occur for observing the upper atmosphere.

### 2.1.1 Science Investigation

The Distributed Radiosonde mission will act as a swarm of sensors to characterize the environment from the upper atmosphere to the surface over a volume of space, as opposed to current radiosonde missions which offer only a singular data point. The following science objectives will be met: 1) Determine the pressure, temperature, relative humidity, and wind conditions throughout the flight; 2) Transmit the collected data to a ground station. The science traceability matrix in Table 2-1 outlines how the science objectives led to the instrument selection.

Table 2-1 – Science Traceability Matrix

| Science Objectives, Expected Outcomes | Scientific Measurements Requirements | Instrument Functional Requirements | Possible Instruments | Mission and Flight Requirements |
|---|---|---|---|---|
| Determine the pressure, temperature, relative humidity, and wind conditions of the upper atmosphere | Detect gas pressure (<=100 kPa). Detect relative humidity (0-100%RH). Measure temperature (-210-300K). Measure wind speeds (0-0.16 km/s). | Active remote sensing of environment between the upper atmosphere and the ground. | BMP 085<br>SHT 15<br>MPXV7002 | Achieve an altitude of 27km, below the launch vehicle maximum (~30 km). Release distributed sensing system into environment. |
| Transmit the collected data to a ground station | Transmit the collected data over amateur satellite radio band | Active transmission of data collected between upper atmosphere and the ground. | CC430 | Process collected data. |

The scientific measurement requirements outline the expected range in measurements from the stratosphere, the region of the atmosphere from 12km to 51km, to the ground. The pressure-sensing unit must be capable of sensing gas pressures below 1 kPa because atmospheric pressure decreases exponentially with altitude, with 90% of the total atmosphere contained within 16km from sea level. Temperatures increase in temperature from 210K at the bottom of the stratosphere (12km) to 270K at the top (51km) due to ultraviolet light absorption in the upper layers of the stratosphere. Below the stratosphere, the troposphere has an increase in temperature with a decrease in altitude. The telemetry design will utilize an amateur radio frequency to transmit the collected data to a ground station. The use of an amateur radio frequency aids in the ability to track the systems from multiple locations throughout the world. The functional requirements describe the necessary functions the instruments must be able to perform to accomplish the mission. The weather sensors must be able to continuously collect data during flight and transmit the data.

These objectives were met by employing instruments suited to measure the desired parameters while keeping the payload mass very small. The BMP-085 from Bosch, shown in Figure 2.1, is a high-precision, ultra-low power digital barometer. It offers a measuring range of 30 to 110 kPa with an accuracy of 0.003 kPa.


Figure 2.1: BMP-085 digital barometer, *Image courtesy of Bosch*

The SHT 15, shown in Figure 2.2, by Sensirion is a surface mountable relative humidity and temperature sensors integrated onto one chip. The device is capable of measuring relative humidity from 0-100% and temperature from 230-390K, and an accuracy of 0.1% and 0.1K respectively.

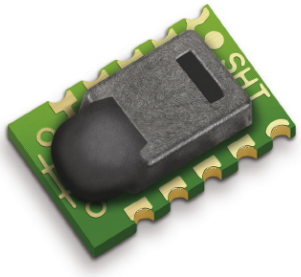


Figure 2.2: SHT 15 relative humidity and temperature sensor, *Image courtesy of Sensirion*

The MPXV7002 in Figure 2.3, from Freescale Semiconductor, is a digital pressure sensor capable of measuring positive and negative pressure. Along with adding redundancy in pressure measurements, this device has a range from -2.0-2.0 kPa. This device can be used to measure the airspeed during descent.

Figure 2.3: MPXV7002 digital pressure sensor, *Image courtesy of Freescale Semiconductor*

The CC430, shown in Figure 2.4, is a microprocessor made by Texas Instruments. The unique feature of the CC430 is the built in, low-power, radio transceiver. The CC430 is not only capable of processing the data from the other instruments, but also serves as the transmitter of the collected information.


Figure 2.4: CC430 microprocessor and low-power RF, *Image courtesy of Texas Instruments*

The total payload suite is displayed in Table 2-2. The entire science payload has a weight of 7 grams, and each sensor can be integrated onto a PCB.

Table 2-2 – Upper Atmosphere Science Payload Suite

| | |
|---|---|
| **Science Instruments** | BMP-085<br>SHT 15<br>MPXV7002<br>CC430 |
| **Payload Mass** | 7 g |
| **Measures** | Pressure (30-110 kPa)<br>Humidity (0-100%)<br>Temperature (230-390K)<br>Airspeed (0-0.15 km/s) |

### 2.1.2 Mission Phases

The Distributed Radiosonde mission is divided into the following mission phases:

1. Launch and Atmosphere Insertion

This phase initiates the Distributed Radiosonde mission with a weather balloon launch. The first stage of the launch system consists of a unit used to deploy the sensing system. The weather balloon will ascend for approximately 100 minutes while it reaches a maximum altitude of about 30 km. Once an altitude of 27 km is reached, the deployment unit will release the individual sensing systems and allow the sensing systems to begin their descent before the balloon bursts from over-expansion.

2. Descent and Operations – Science Acquisition

The goal of this phase is to fulfill the science objectives and mission requirements. The distributed sensing system will descend through the atmosphere to collect data. The collected data will be processed and transmitted over an amateur radio frequency. During descent, the vehicle will self stabilize and auto-rotate to generate lift to increase the exposure time to the environment.

3. End of mission

The individual systems will continue to collect and transmit data until the gently land on the ground, where they will continue to transmit a signal for potential recovery purposes or until power is lost.

## 2.2 Vehicle Concept Development

The vehicle design philosophy focused on creating an effective test vehicle. The systems were chosen to maximize simplicity in the design and minimize cost. The design process focused primarily on developing a system with which to demonstrate operation feasibility rather than focusing on the optimization the vehicle itself.

### 2.2.1 Samara Craft Architecture

The flight system design for the samara craft includes the flight system requirements, the samara craft architecture and design models. The flight system requirements summarize the capabilities that each subsystem needs to uphold in order to accomplish the mission. The samara craft architecture includes all the necessary subsystems needed for the craft to operate. The launch vehicle being used is a 60-gram weather balloon with a main payload box that will house the samara crafts. Several design models were created to assist in the design of the individual samara crafts.

The flight system requirements for the samara craft mission include the general constraints for each vehicle system.

- The vehicle must be small and light enough in order to conform to the capability of reentry from LEO without harmful thermal loads.
- The vehicle geometry must be capable of generating the necessary aerodynamic forces to maintain a stable orientation during descent.
- The payloads must be exposed to the environment to capture atmospheric measurements.
- The vehicle must be capable of transmitting the data recorded to a ground station.

Each samara craft will contain an identical payload suite. This payload suite will include

the instruments defined in the science investigation. These instruments will be arranged on a single PCB along with the other components necessary to operate the craft. Because of the unique design of the sensing systems, several traditional subsystems can be neglected. For example, because of the vehicle's ability to passively generate lift and provide a stable orientation, an active propulsion system is not required.

The CC430 is a low power microprocessor that can be used for command and data handling. The device is capable of receiving and processing information from sensors, as well as handle commands. Power will be supplied from a small Polymer Lithium-ion battery. This lightweight battery operates at 110 mAh and 3.6V, and is suitable for use with small electronic devices.

A process called code division multiple access (CDMA) applied to this specific distributed space mission is being investigated to allow for simultaneous transmission of information on the same frequency. This modulation scheme will allow each sensing system to share a common frequency. A key design feature of the CC430 microprocessor is that it contains a built-in software defined radio, capable of transmitting and receiving signals. This integrated chip can be used to handle the communication requirements. An active antenna is also needed to complete the subsystem design.

The attitude determination and control subsystem stabilizes the vehicle and orients it in the necessary directions required during the mission despite the external disturbances acting on the craft. Because of the unique geometry of the sensing system, a stable attitude is achieved passively without the need for sensors to calculate the orientation.

## 2.3 Samara Flight Theory

A minimized descent rate as well as a stable flight orientation depends on the proper flight operations of the samara vehicle being developed. Because lift and stability is being generated passively, a detailed investigation into the overall flight and stability characteristics was needed in order to fully understand and implement the geometry of a samara into the prototype design.

### 2.3.1 Single-Wing Samara

This geometry is typical of maple and ash trees. These samaras have a seed mass at one end and have a ribbed structure that improves the aerodynamics via surface roughness and keeps the center of gravity forward.

As a samara falls, the offset between the gravity acting at the center of mass and the resultant drag force creates a yawing moment. The offset results in a tilted equilibrium orientation where a chordwise flow is generated over the span of the seed's wing. This chordwise flow and yaw rate induce aerodynamic and inertial forces, which further accelerate the spin of the samara. The spin is centered about a point near the center of mass near the seed, while the wing tip traces a helical shape during descent. This motion is known as autorotation and is self-stabilizing, and is characterized by the extraction of energy from the airflow over the rotating blade, and utilizing this energy to sustain the rotation and generate thrust.

There have been several studies regarding the biological function of samaras, but Norberg conducted the first major study regarding the flight mechanics of autorotating samaras. He performed experiments using thin, flat plate models to examine the autorotational descent of a samara. Norberg investigated how momentum theory could be

applied to describe the aerodynamic interactions of autorotation, analyzed of the stability characteristics during autorotation, and also briefly investigated the effects of the samara geometry on its flight performance. Figure 2.5 represents the leading edge of a samara during steady state autorotational descent and the forces acting on it.

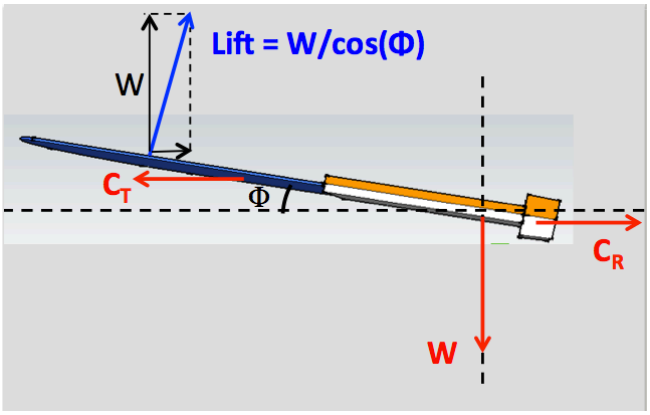


Figure 2.5: Free body diagram of a Samara vehicle

The resultant lift force over the span of the wing is shown acting on the samara's overall center of pressure, while the weight force due to gravity is shown acting at the center of mass. During autorotational descent, the vertical component of the lift force is equal in magnitude to the weight of the samara. Two centrifugal forces act on either side of the samara at specified spanwise locations. For a particular descent rate and rotation rate, the balance of these forces determines the center of rotation. Also, the moments created by lift and centrifugal forces about the center of mass create an equilibrium condition such that there is a constant angle between the spanwise axis and the local horizontal, phi, which is referred to as the coning angle. The horizontal component of the lift force remains, and tends to accelerate the wing of the samara inward; however, the direction of this force varies rapidly, and its effect is treated as negligible [18].

In autorotation descent, the samara possesses both static and dynamic stability. A

balance of the above mentioned forces provides stability of the pitching plane, or feathering plane, which involves a combination of a stable angle of attack and a stable gliding angle, stability on the coning plane, or flapping plane, as well as directional stability, which is stability of the angle of the wing tip path plane relative to the horizontal during descent.

### 2.3.2 Flying Wing Body Samara

The *alsomitra macrocarpa*, or Javan cucumber, is commonly found in Southeast Asian forests and grows samaras that consist of a paper thin, flying wing structure around a flattened seed and are able to glide smoothly for long periods of time without an active stabilizing system. Figure 2.6 shows the naturally occurring samara.

Figure 2.6: Alsomitra macrocarpa

As the seed descends, the air moving over the wings generates a lifting force. The lift acts slightly forward of vertical because the seed is descending. This horizontal component of the lift is enough to overcome the induced drag forces and allows the glider to accelerate forward. Although flying wing bodies lack stability around the vertical and lateral axes, the *alsomitra macrocarpa* seed achieves stability through particular geometric features. The result is the seed achieves phugoid flight with a glide ratio of 8:1.

Reflexed trailing edges are perhaps the most complex of the stabilizing features on flying wing aircraft. Most airfoils have a camber line that is concave down. Wings with a

reflexed trailing edge have a camber line that changes concavity, making the camber line near the trailing edge have an upwards concavity. This change in camber reduces the pitch-up tendencies of flying wing aircraft and reduces the likelihood of stall.

Dihedral is the angling of the wings upward as viewed from a frontal perspective of the craft. This provides lateral stability, like wing sweepback. Because the wings are angled, their lift vectors are also angled. When the aircraft is banked, the lower wing will have a higher vertical component of lift than the upper wing, creating a torque about the longitudinal axis, which returns the plane to equilibrium.

Sweepback on a small scale produces three stabilizing effects. When sideslip is induced, a swept wing will tend to produce a rolling moment reaction as to reduce the angle of sideslip. This occurs as a result of the effective change in flow direction over the wing due to the relative sweep angles being different. The net result reduces to dominance of the spiral mode in the lateral response. Sweepback also provides some directional stability: if the craft is yawed, the wing opposite the direction of yaw experiences an increase in frontal area, which increases parasite and induced drag for that wing while reducing in drag on the other wing. These forces produce a torque about the vertical axis returning the craft to its original orientation. In flying wing aircraft, sweepback also provides longitudinal stability. In conventional aircraft, longitudinal stability is provided by the horizontal stabilizer, which generates negative lift. The horizontal stabilizer is placed at such a distance from the center of gravity of the craft so that it produces a moment equal and opposite to the moment created by the lift of the wings. A flying wing does not have a horizontal stabilizer, but the sweep back of the wings is usually sufficient such that the wingtips are far enough behind the center of gravity to have effective leverage and act as a

horizontal stabilizer.

### 2.3.3 Geometry Design

With a general understanding of the flight behavior, an open source 3D CAD software was used to conceptually design the samara geometries. Figures 2.7 and 2.8 show the CAD designs created. These designs optimally place the payloads in such a way as to induce stability during flight.

A decision to use the single wing geometry was made. This decision was driven by the mass of the science payload. It was determined that for a payload mass of 7 grams, the flying wing body samara would require a large surface area wing to be designed. Creating dihedral at the wing tips was also a difficult manufacturing challenge. The single wing samara design was based on a flat plate with a thick leading edge. This design was simple to rapidly manufacture. With a vehicle architecture and geometry chosen, the next step was to analytically model the flight of the chosen prototype vehicle. This work is presented in Chapter 3.

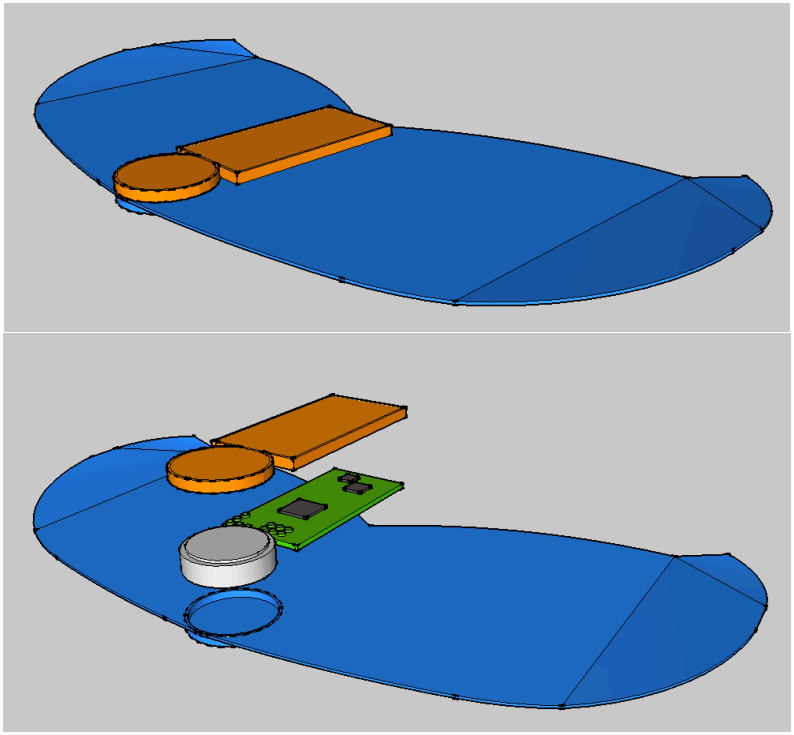

Figure 2.7: Flying wing geometry design, isometric and exploded view

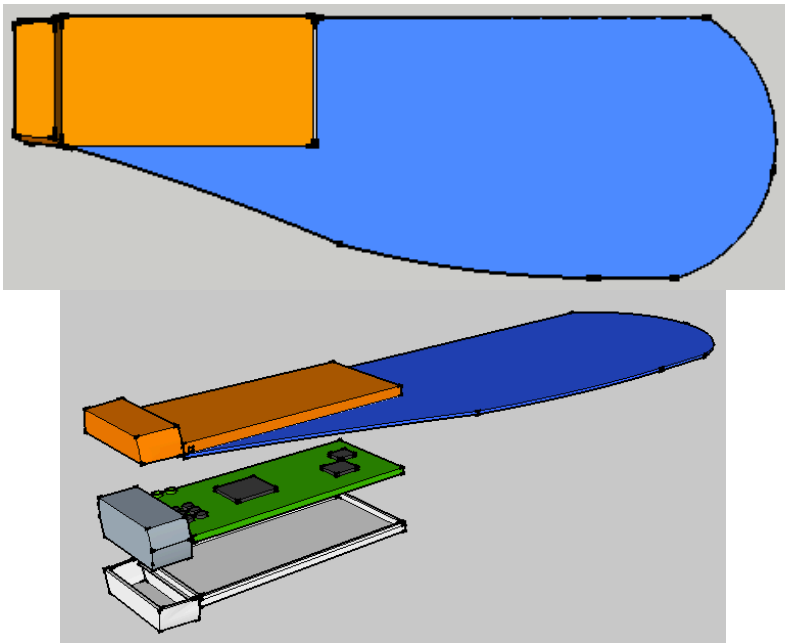

Figure 2.8: Single wing geometry design, top and exploded view

# CHAPTER 3

# DYNAMIC SIMULATION

The goal of this analysis is to better understand the steady state flight behavior of a samara. First an analytic model describing the samara's behavior was formulated. Then a time-domain simulation was created with the ability to numerically solve this analytical model.

## 3.1 Analytic Model

The first step in creating the simulation was the development of an analytical model to describe the vehicle's dynamics and aerodynamics. This analytical model splits into two categories: the equations of motion that describe the six-degree-of-freedom rigid body dynamics of the samara, and the equations governing the external forces and moments generated by aerodynamic interactions [19, 20].

### 3.1.1 Equation of Motion

During flight, the samara can be treated as a fully unconstrained rigid body that is free to translate and rotate in all six degrees of freedom. To model this type of motion, a standard formulation for the rigid body motion of a spacecraft was used from Wiesel. To do this, two reference frames were defined: the body frame was attached to the vehicle, with the origin located at the center of mass (CoM) of the vehicle; the inertial frame was used to define the body frame's location in space. This relationship is shown in Figure 3.1.

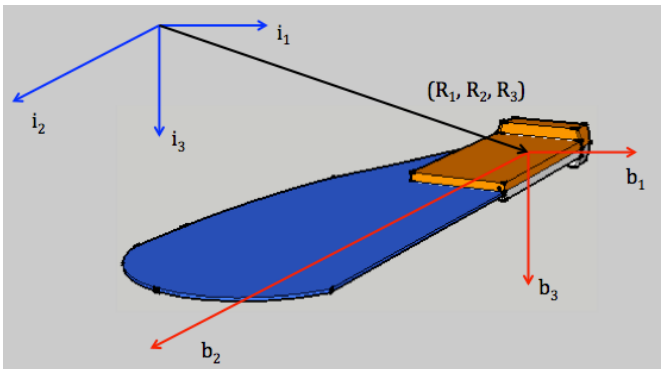


Figure 3.1: Inertial and body-fixed reference frames

Euler angles were used to describe the orientation of the body frame in the inertial frame. The three individual rotations were performed sequentially to re-orient the body frame:

a. Rotate by $\psi$ about $\widehat{i_3}$ to get $(b_1', b_2', b_3')$

b. Rotate by $\theta$ about $\widehat{b_2'}$ to get $(b_1'', b_2'', b_3'')$

c. Rotate by $\phi$ about $\widehat{b_1''}$. This results in $(b_1, b_2, b_3)$

The Euler angles are $\phi$, $\theta$, and $\psi$, which are also known as roll, pitch, and yaw respectively in aircraft terminology. The above rotation sequence is known as the 3-2-1 sequence because of the labeling of the axes about which rotation occurs. The use of Euler angle rotations results in singularities when a rigid body reaches a particular orientation. The singularity associated with the 3-2-1 sequence occurs when $\theta = \pi/2$, when rotation about phi and psi cannot be distinguished from one another. This singularity did not pose a problem for the modeling of the samara, because stable flight conditions of a descending samara have relatively low pitch angles.

The rotation sequence can be represented in matrix form, called the direction cosine matrix.

$$C(\Theta) = \begin{bmatrix} \cos\psi & \sin\psi & 0 \\ -\sin\psi & \cos\psi & 0 \\ 0 & 0 & 1 \end{bmatrix} \begin{bmatrix} \cos\theta & 0 & -\sin\theta \\ 0 & 1 & 0 \\ \sin\theta & 0 & \cos\theta \end{bmatrix} \begin{bmatrix} 1 & 0 & 0 \\ 0 & \cos\phi & \sin\phi \\ 0 & -\sin\phi & \cos\phi \end{bmatrix} \tag{3.1}$$

where:

$$\Theta = \begin{bmatrix} \phi \\ \theta \\ \psi \end{bmatrix} \tag{3.2}$$

Performing the matrix multiplication yields:

$$\mathrm{C}(\Theta) = \begin{bmatrix} \cos\theta\cos\psi & \cos\theta\sin\psi & -\sin\theta \\ -\cos\phi\sin\psi + \sin\phi\sin\theta\cos\psi & \cos\phi\cos\psi + \sin\phi\sin\theta\sin\psi & \sin\phi\cos\theta \\ \sin\phi\sin\psi + \cos\phi\sin\theta\cos\psi & -\sin\phi\cos\psi + \cos\phi\sin\theta\sin\psi & \cos\phi\cos\theta \end{bmatrix} \tag{3.2}$$

The complete transformation from body to inertial frame can be represented by the following equation:

$$\begin{bmatrix} \widehat{b_1} \\ \widehat{b_2} \\ \widehat{b_3} \end{bmatrix} = \mathrm{C}(\Theta) \begin{bmatrix} \widehat{\imath_1} \\ \widehat{\imath_2} \\ \widehat{\imath_3} \end{bmatrix} \tag{3.3}$$

The next step is to find the three coupled differential equations for the time rate of change of the Euler angles. These equations relate the angular velocity components to the Euler time derivatives. To do this, the following S matrix is defined:

$$S = \begin{bmatrix} 1 & 0 & -\sin(\theta) \\ 0 & \cos(\phi) & \sin(\phi)\cos(\theta) \\ 0 & -\sin(\phi) & \cos(\phi)\cos(\theta) \end{bmatrix} \tag{3.4}$$

This S matrix allows us to form the three equations in matrix form. The angular velocity of the samara is:

$$\omega = S\dot{\Theta} \tag{3.5}$$

Making the Euler angle time derivatives:

$$\dot{\Theta} = S^{-1}\omega \tag{3.6}$$

where:

$$S^{-1} = \begin{bmatrix} 1 & \sin\phi\tan\theta & \cos\phi\tan\theta \\ 0 & \cos(\phi) & -\sin(\phi) \\ 0 & \sin\phi\sec\theta & \cos(\phi)\sec\theta \end{bmatrix} \tag{3.7}$$

By investigating the SINV matrix, the singularity associated with the 3-2-1 sequence becomes apparent. At $\theta = \pi/2$, the $S^{-1}$ matrix becomes undefined. Equation 3.6 can now be integrated to yield the orientation.

The following state vector X is assembled:

$$\mathbf{X} = \begin{pmatrix} \omega \\ \Theta \\ \mathrm{V} \\ \mathrm{R} \end{pmatrix} \tag{3.8}$$

This vector fully describes the position, orientation, translational rate, and rotational rate of the vehicle. The position and velocity quantities, denoted R and V, are refer to the origin of the body frame, located at the CoM of the vehicle. The individual components of the state vector are as follows:

$\omega$: roll, pitch, and yaw rate of the vehicle in the body frame:

$$\omega = \begin{bmatrix} \omega_1 \\ \omega_2 \\ \omega_3 \end{bmatrix} \tag{3.9}$$

$\Theta$: roll, pitch, and yaw of the vehicle in the body frame:

$$\Theta = \begin{bmatrix} \phi \\ \theta \\ \psi \end{bmatrix} \tag{3.10}$$

V: velocity of the body frame relative to the inertial frame, expressed in body frame:

$$\mathrm{V} = \begin{bmatrix} V_1 \\ V_2 \\ V_3 \end{bmatrix} \tag{3.11}$$

R: position of the body frame relative to the inertial frame, expressed in body frame:

$$\mathrm{R} = \begin{bmatrix} R_1 \\ R_2 \\ R_3 \end{bmatrix} \tag{3.12}$$

The following is the formulation of the scalar equations of motion, where external forces

and moments are represented by the variables F and M respectively. In finding the time rate of change of velocity, the equation of linear momentum is:

$$\dot{\mathrm{P}} = -\omega\times\mathrm{P} + \mathrm{F} \tag{3.13}$$

where:

$$\mathrm{P} = m\mathrm{V} \text{ and } \dot{\mathrm{P}} = m\dot{\mathrm{V}} \tag{3.14}$$

Substituting the above relation yields:

$$m\dot{\mathrm{V}} = -m\omega\times\mathrm{V} + \mathrm{F} \tag{3.15}$$

$$\dot{\mathrm{V}} = \frac{\mathrm{F}}{m} - \omega\times\mathrm{V} \tag{3.16}$$

To find the time rate of change of angular velocity, we need the angular equation of motion:

$$\dot{\mathrm{H}} = -\omega\times\mathrm{H} + \mathrm{M} \tag{3.17}$$

where:

$$\mathrm{H} = \mathrm{I}\omega \text{ and } \dot{\mathrm{H}} = \mathrm{I}\dot{\omega} \tag{3.18}$$

Substituting equation 3.18 into 3.17 yields:

$$\mathrm{I}\dot{\omega} = -\omega\times\mathrm{I}\omega + M \tag{3.19}$$

$$\dot{\omega} = \mathrm{I}^{-1}(-\omega\times\mathrm{I}\omega + M) \tag{3.20}$$

The final expressions of equations 3.16 and 3.20 can be integrated to yield V(t) and $\omega$(t). The final equation is the kinematic equation for the time rate of change of position:

$$\mathrm{V} = \dot{\mathrm{R}} + \omega\times\mathrm{R} \tag{3.21}$$

which yields:

$$\dot{\mathrm{R}} = \mathrm{V} - \omega\times\mathrm{R} \tag{3.22}$$

Equation 3.22 can now be integrated to find R(t), which is expressed in the body frame. The solution can be subsequently transformed into the inertial frame.

### 3.1.2 Aerodynamic Model: BEMT

The external forces and moments mentioned above must be considered to complete the analytical model of the samara vehicle. These forces and moments consist of gravitational disturbances and aerodynamic interactions with the surface of the vehicle. The rotation of a samara can be compared to that of a conventional helicopter rotor blade. The major difference is that the samara is mechanically unconstrained. Because of the aerodynamic similarities between the samara and a conventional rotor blade, classical blade element momentum theory (BEMT) can be used to model the aerodynamics of a samara.

BEMT is a combination of blade element theory and momentum theory. Momentum theory was developed on the basis that a spinning rotor could be modeled as an actuator disc. This disc uniformly changes the speed of the air passing through it, and the thrust required is represented by the axial kinetic energy imparted to the air composing the slipstream [21]. The change in velocity of the air from the initial value to the value at the rotor disc is known as the induced velocity, $v_i$. Figure 3.2 illustrates the flow model for momentum theory.

Blade element theory takes into consideration the contribution of many 2-dimensional slices of the rotor blade. This provides a model that estimates the radial and vertical variations in aerodynamic loading over the entire rotor disc. This theory treats each element as a 2-D airfoil section that produces forces and moments independently of other elements. The thrust and torque of the rotor are obtained by integrating the individual contribution of each element along the length of the blade. An example of a blade element's lift and drag contribution can be seen in Figure 3.3.

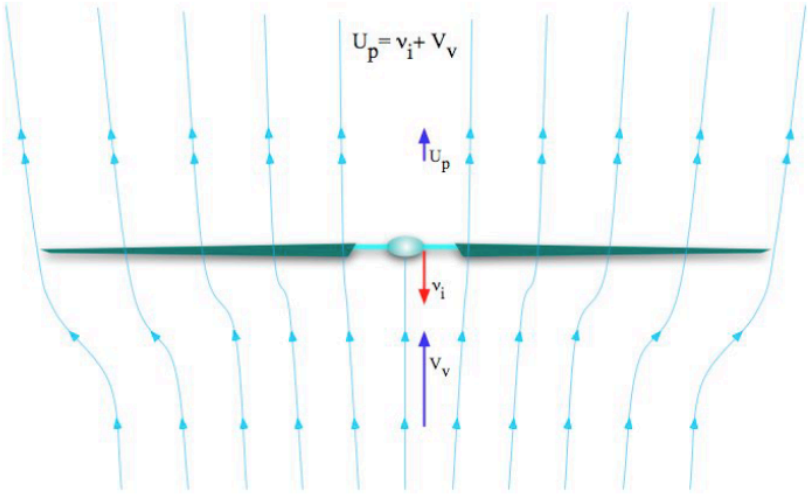


Figure 3.2: Flow model for momentum theory analysis of a descending rotor [22]

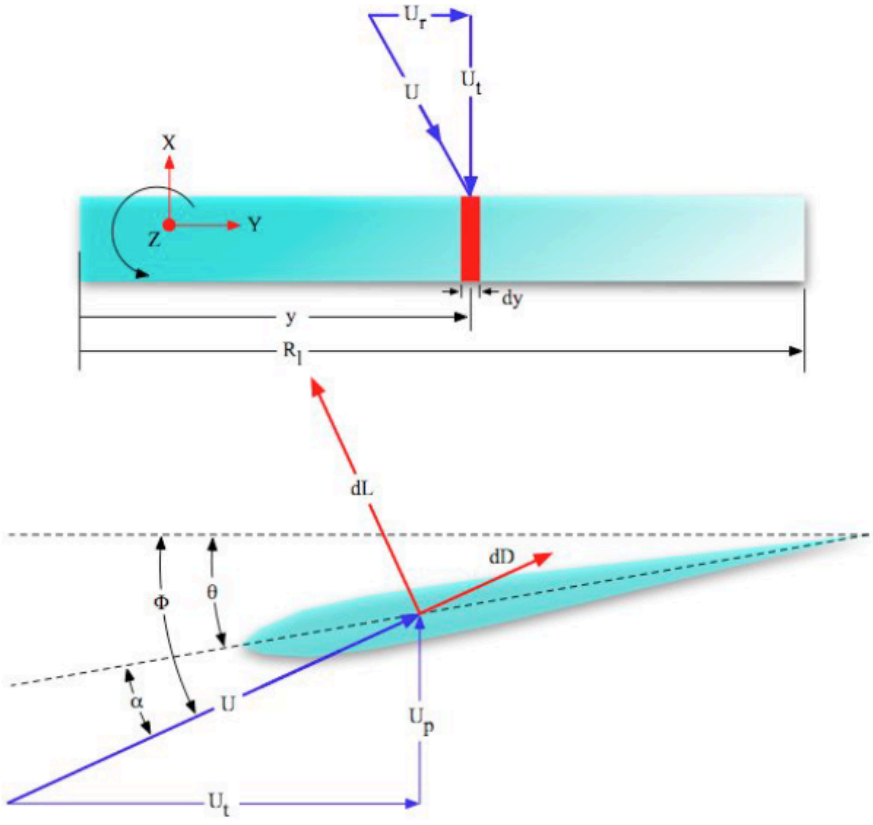


Figure 3.3: Blade element analysis airflow and resulting lift and drag forces [22]

As a hybrid of the two theories, BEMT states that the momentum theory of lift is equivalent to the circulation theory, which allows for the calculation of the distribution of

induced flow along the blade. The direct result of combining momentum theory and blade element theory is that momentum considerations are applied to an annulus of a rotor disc. This formulation is used to calculate the external forces and moments of the samara vehicle.

The following assumptions were made when formulating the equations to describe the aerodynamics. Model describes a samara in steady-state autorotation motion. The following initial conditions must be used: a non-zero descent rate, a non-zero yaw rate, and an orientation that represents steady-state autorotation. The vehicle is operating in a windmill brake state. As shown in figure 3.1.2, the windmill brake state is a case where the induced velocity causes a decrease in the velocity of the airflow as it approaches and passes through the rotor disc, causing the slipstream to expand above the disc. It was assumed that the conditions outlined for the 2-dimensional BEMT model would be sufficient to describe the model. Therefore, 3-D effects such as tip losses were not considered. Finally, a Reynolds number on the order of $10^4$ was considered for this model. This Reynolds number describes the conditions that the samara vehicle would experience towards the end of its flight, where atmospheric conditions approach and equal sea level conditions. The model demonstrates the reduced descent rate at this stage in flight to provide for a gentle landing and recovery.

The coordinate system being used is equivalent to the body fixed coordinate mentioned previously. The model begins by focusing on a single 2-D blade element. To obtain an expression for the induced flow, the derivation presented by Gessow and Meyers was used, and summarized here. For a particular blade element, the vertical component of velocity is computed by subtracting the velocity at the element due to the vehicle's roll

from the vehicle's descent rate:

$$V_v = -v_3 - \omega_1(r - \mathrm{CM}_y) \tag{3.23}$$

where:

$$r = y\mathrm{R}_l \tag{3.24}$$

To obtain an expression for induced flow, blade element theory is used to form an expression for the differential thrust produced by a blade element:

$$dT = b\frac{1}{2}\rho(\omega_3 r)^2 a(\theta - \Phi)cdr \tag{3.25}$$

Next, momentum theory is used to form an expression for differential thrust of an annulus:

$$dT = 4\pi\rho u v_i r dr \tag{3.26}$$

These two expressions for differential thrust are set equal to one another, and the resulting quadratic expression is used to solve for induced velocity to yield:

$$v_i = \left(\frac{V_v}{2} + \frac{\sigma a \omega_3 r}{16}\right)\left(-1 + \sqrt{\frac{2(\theta r \omega_3 - V_v)}{\frac{4{V_v}^2}{\sigma a \omega_3 R} + V_v + \frac{\sigma a \omega_3 r}{16}}}\right) \tag{3.27}$$

Equation 3.27 can now be used to compute the induced flow at the blade element. Knowing the vertical velocity due to vehicle motion and the induced flow velocity, the resultant vertical velocity at the element can be computed:

$$U_p = v_i + V_v \tag{3.28}$$

Now the resultant tangential velocity at the blade element can be computed. The tangential velocity is composed of the lateral translation of the vehicle in the b1 direction and the velocity due to the spinning of the wing:

$$U_t = -\omega_3\left(r - CM_y\right) - v_1 \tag{3.29}$$

The above expressions are used to find the total resultant velocity:

$$U = \sqrt{{U_p}^2 + {U_t}^2} \tag{3.30}$$

The angle between the resultant velocity vector and the horizontal can be computed:

$$\Phi = \tan^{-1}\left(\frac{U_p}{U_t}\right) \tag{3.31}$$

The blade element's angle of attack is found by adding the resultant velocity's vector angle with the pitch angle:

$$\alpha = \Phi - \theta \tag{3.32}$$

Knowing the angle of attack, the lift and drag coefficients of the blade element can be determined. This data depends on the airfoil being presented in the model. During the course of this analysis, the airfoil represented was a flat plate. Flat plate wind tunnel data for high angles of attack were obtained from NACA Technical Report 3221 and the results are shown in Figure 3.4.

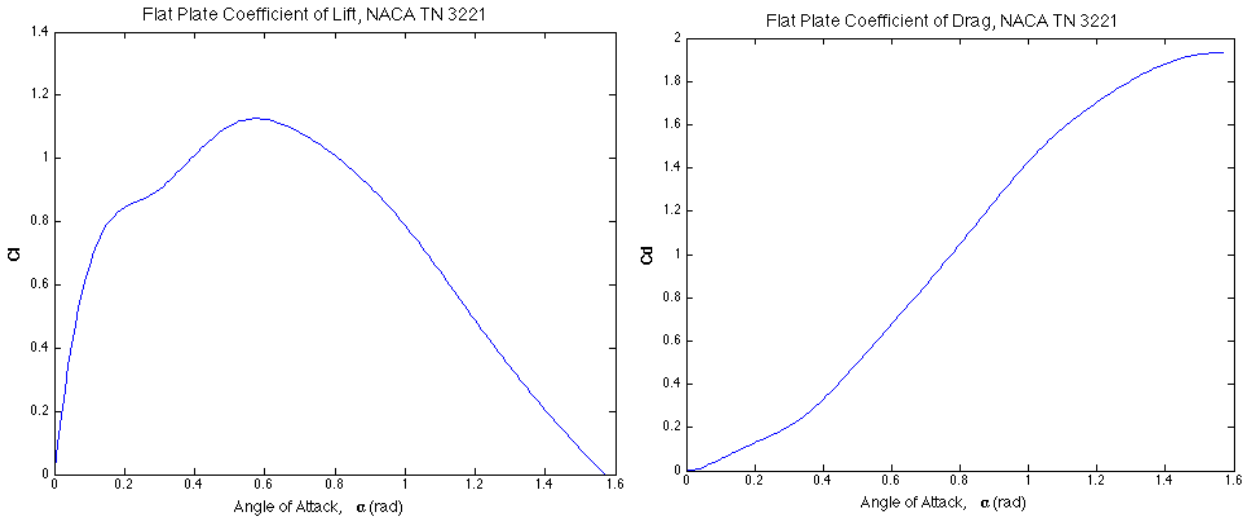


Figure 3.4 Coefficients of lift and drag as a function of angle of attack for a flat plate

Using the lift and drag coefficients, the lift and drag produced by the element is found:

$$dL = -\frac{1}{2}\rho U^2 c C_l dr \tag{3.33}$$

$$dD = -\frac{1}{2}\rho U^2 c C_d dr \tag{3.34}$$

Lift is generated normal to the resultant air velocity experienced by an airfoil, while drag is parallel to the air velocity. The lift and drag forces must be rotated into the body frame, because the samara model specifies external forces and moments in the body frame. This relationship is illustrated in figure 3.5. This results in the formulation of the normal and axial forces experienced by the blade element:

$$dN = dL\cos\alpha + dD\sin\alpha \tag{3.35}$$

$$dA = -dL\sin\alpha + dD\cos\alpha \tag{3.36}$$

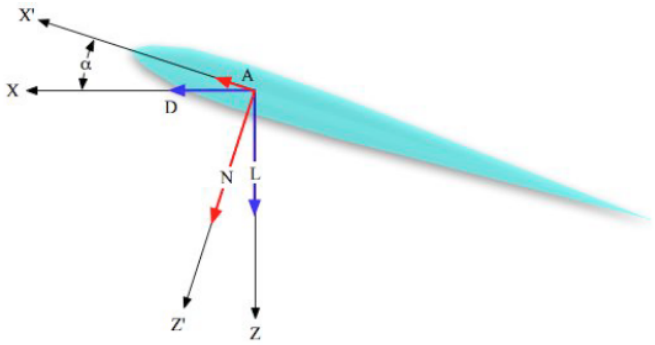


Figure 3.5 Rotation of lift and drag into body frame to get normal and axial forces [22]

Once the normal and axial forces are obtained, the rolling, pitching, and yawing moments generated by the individual blade element can be computed. The moment arm used depends on the radial distance of the particular blade element from the vehicle's CoM location. The expressions for the aerodynamic moments are:

$$M_x = N(r - CM_y) \tag{3.37}$$

$$M_y = N(CM_x) \tag{3.38}$$

$$M_z = -A(r - CM_y) \tag{3.39}$$

Once the forces and moments are found, the process is repeated until all of the blade

elements have been calculated. The forces and moments are then integrated over the span of the samara. These values are then passed to the dynamic loop as external forces and moments.

## 3.2 Free-flight Simulation Development

With the analytical model complete, a time domain computer simulation was created to numerically solve the model's equations. This simulation was implemented in MATLAB, and was programmed as several individual functions. The simulation contained all the necessary equations of motion and aerodynamic contributions to model the samara in free-flight descent. Figure 3.6 illustrates the individual functions and the data-flow between them.

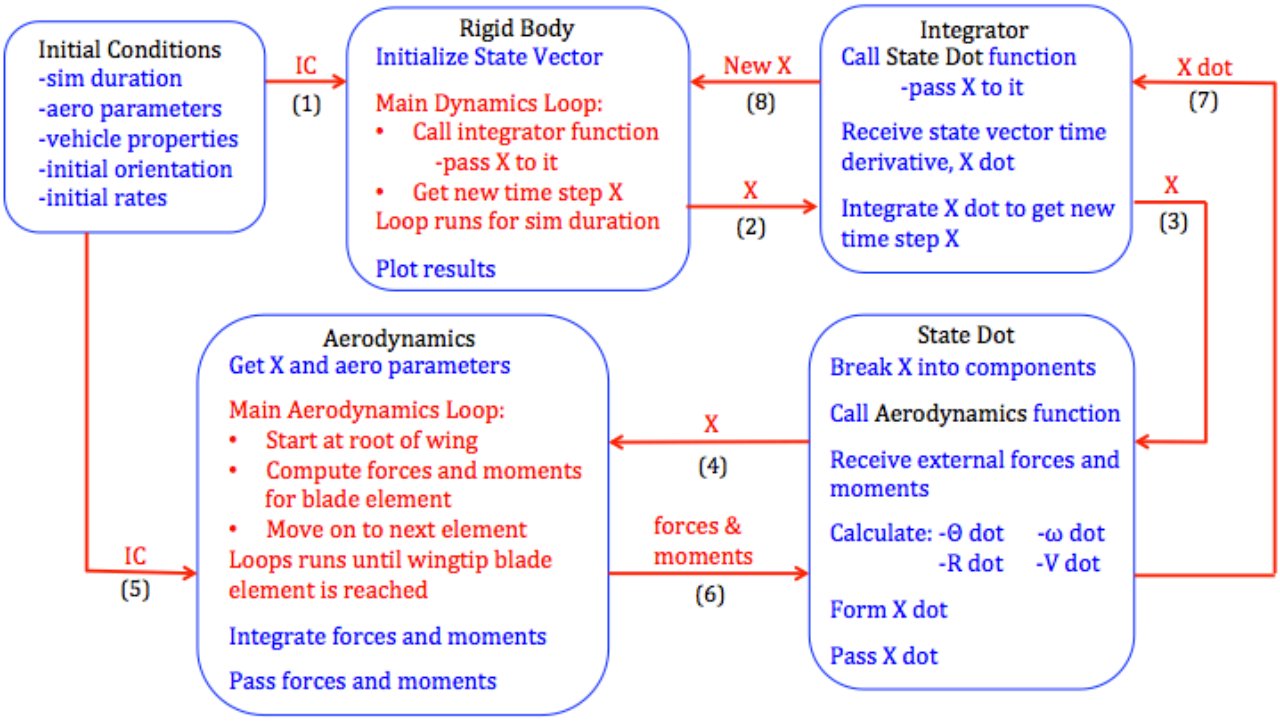


Figure 3.6 Free-flight simulation block diagram

A study conducted by H.S. Morton involved a 4-Euler parameter, rigid body simulation, with numerical results [23]. The same mass properties were used in a

verification of the Rigid Body function developed above. The simulation of just this function matched the results from Morton's study, verifying the proper functioning of the Rigid Body main dynamics loop. The goal of the free-flight simulation was to analytically predict the descent rate and spin rate of a samara shaped vehicle. This entire simulation (in particular the Main Aerodynamics Loop) was validated by comparing results to flight tests of a model samara. The results are presented in Chapter 4.

# CHAPTER 4

# SIMULATION VALIDATION AND PROTOTYPE TESTING

With the simulation complete, the testing of free flight samaras was conducted. The goal for this field experiment was to validate the simulation results. Two different free-flight iterations were designed, constructed, and test flown. The resulting flights were captured on video from multiple perspectives. A vehicle's descent rate and rotation rate could be determined by analyzing the video data. The second iteration prototype also featured a sensor unit capable of measuring magnetic field strength, acceleration, and orientation. The operation of this inertial measurement unit will be discussed in detail in the Second Iteration section.

## 4.1 First Design

The first samara prototype was designed to resemble a natural maple seed. This included a thin flat plate for a wing, a stiff leading edge, and a dense payload connected to one end of the leading edge. The wing planform included a taper at the root, which is seen in maple seeds. Figure 4.1 depicts the first prototype. The wing section was fabricated from 0.35mm thick birch wood. The main spar of the leading edge was made out of 1 mm diameter copper wire with thin rubber insulation. The payload was formed to mimic the mass of a small PCB with a battery at the end.

Figure 4.1: Birchwood samara prototype model

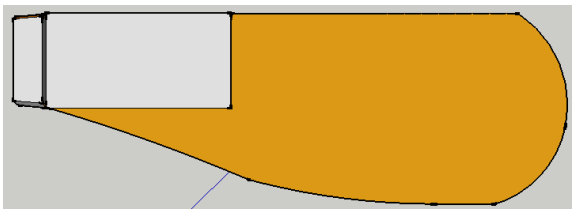

Figure 4.2: CAD drawing of samara prototype model

The fabricated vehicle had a total span of 12.65 cm, a root chord of 2.5 cm tip chord of 4.41 cm, and a total mass of 9.5 grams. The CoM location and inertia matrix of the vehicle during its initial flight tests were determined using the solid model in Figure 4.2. The CoM location was found in the body frame coordinates, shown in Figure 4.3.

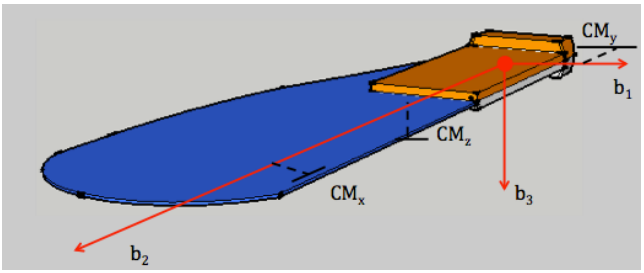


Figure 4.3: Center of mass location in body-fixed coordinates

The length and mass properties associated with the prototype vehicle are part of the initial conditions needed for the simulation. The other initial conditions required by the simulation included an initial yaw rate of 5 rad/sec, an initial pitch angle of -0.1 rad, and all other conditions be set to zero. The simulation was conducted for time duration of 8 seconds. The resulting plots, shown in Figure 4.4, show the simulation-predicted descent rate and spin rate. The results indicate a steady descent rate of 3.1 m/s and a steady yaw rate, or spin about the Z-axis of 18.8 rad/sec (180 rpm).

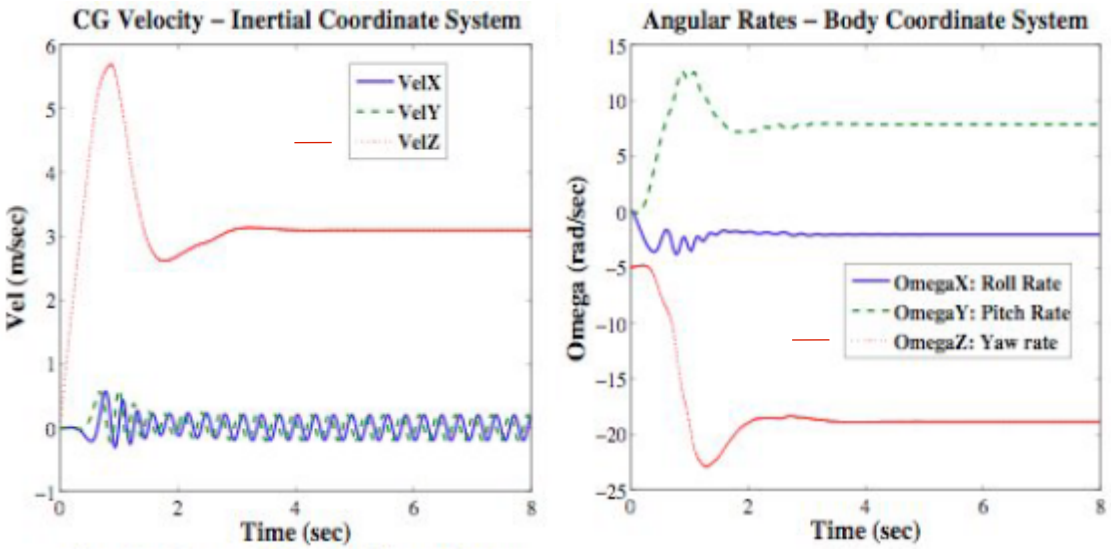


Figure 4.4: Free-flight simulation results with vehicle specifications and initial conditions mentioned above

The prototypes were then test flown in a field experiment. The test vehicle was dropped from the second floor track of the Maverick Activities Center. The recorded video was analyzed to determine the flight performance of the vehicle. A sample screen shot of the video data and the field experiment are shown in Figure 4.5.

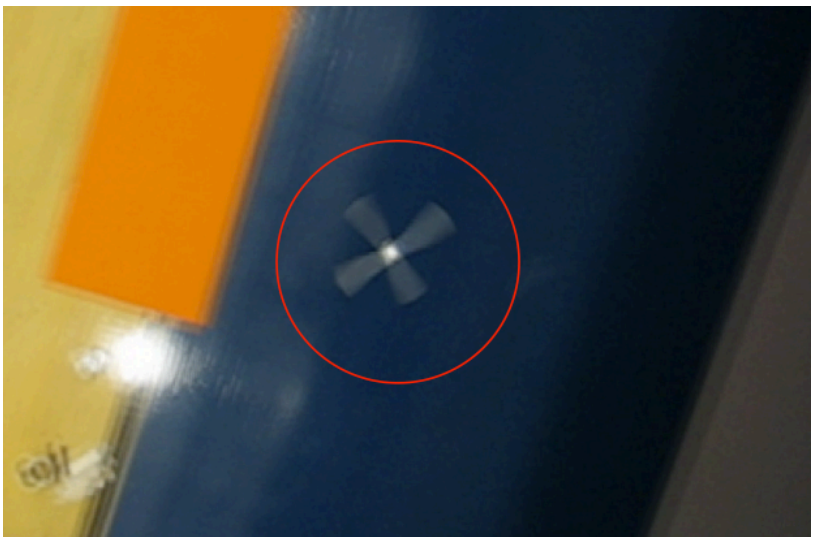

Figure 4.5: Top view screenshot of video data recorded during samara prototype flight tests

Table 4-1 presents a comparison between the experimental data collected and the

simulation predictions of the first samara prototype.

Table 4-1 – Comparison between Calculated and Measured Results

| Parameter | Calculated Results | Experimental Results | Percent Deviation |
|---|---|---|---|
| $U_z$ (m/s) | -2.81 | -2.5 | 12.4 |
| $\omega_z$ (rad/sec) | 18.8 | 16.7 | 12.6 |
| $\theta$ (deg) | 22.8 | - | - |

The simulation has the capability of predicting the steady state roll, or coning angle, that the samara vehicle would experience. The collected experimental data did not provide a means for accurately determining the coning angle. A qualitative assessment of the video data determined that the coning angle was reasonably low enough to not cause unsteady behavior. The errors observed when comparing the simulation flight tests with the experimental data were considered reasonable, and are most likely associated with the lift and drag data used for the simulation. The airfoil's lift, drag, and center of pressure properties used in the simulation were that of a flat plate, and it was hypothesized that the addition of a leading edge spar created the error.

Modified prototypes were designed with the intention of obtaining better correlation with the simulation results. The main change was to use a true flat plate airfoil. The leading edge spar and taper were also removed from this modified design. Identical payload masses were used in both designs. Figure 4.6 shows the modified design.

Figure 4.6: Modified samara prototype design

The resulting design had the same wingspan of 12.65 cm, chord of 4.41 cm, and a total mass of 10.0 grams. The CoM location along the wingspan remained the same, but the chord-wise mass distribution shifted without the concentrated mass of the spar at the leading edge. When attempting to fly this modified design, it was noticed that the spin rate was lower and the coning angle and descent rate were larger before landing, which could lead to unstable conditions if it descended further.

The modified design dimension and mass properties were then entered into the simulation to compare with the modified design's experimental data. Correlation with the simulation also did not improve. Despite the errors indicated in Table 4-1, it was decided that the simulation provided enough fidelity to perform the intended task of predicting the descent performance of the samara vehicle. Work would then progress towards creating a second prototype design that involved collecting real-time data during the descent.

## 4.2 Second Design

The second samara prototype design considered several changes to the original design, in particular the payload and implementation of a lighter "membrane" structure for the wing. The second iteration took a form more closely resembling the nominal design. The expected payload for a distributed mission will be contained on a PCB. Wing designs that are rigid yet lighter than solid counterparts will be utilized to save mass while maintaining the same level of performance.

In an effort to gain real-time flight performance data, a sensing unit was designed to serve as the payload mass for the second prototype. The incorporation of this integrated circuit unit served two purposes: accurate measurement of the flight characteristics of the

vehicle during its descent, and feasibility of recording real-time data that could potentially be transmitted to a ground station. The sensing unit was in fact three separate sensors integrated onto one PCB, available from Sparkfun Electronics. The unit consisted of a 3-axis accelerometer, 3-axis gyroscope, and a 3-axis magnetometer, and together formed a 9 degree-of-freedom inertial measurement unit (IMU). The PCB contained a microprocessor onboard capable of sampling and outputting data at 50 Hz, which is a fast enough resolution to measure the predicted spin rate of 18.8 rad/sec, or 8 Hz. The microprocessor also handled the data from the three sensors and digitally output the information at a baud rate of 9600. A data-logging unit was attached to the IMU to record the raw output from the individual sensors. The logging device saved the recorded data to a micro SD card, for easy access to the logged information. The data-logging device was programmed in such a way that each reset of the IMU board would generate a new file on the memory card and begin recording in the new file. This allowed for a simple method of identifying each flight tests. Finally, a lithium ion battery was used as a power supply. The total weight of the sensing unit, depicted in Figure 4.7, was 9.5 grams. The overall dimensions of the unit were 2.9 cm × 4.1 cm × 1 cm.

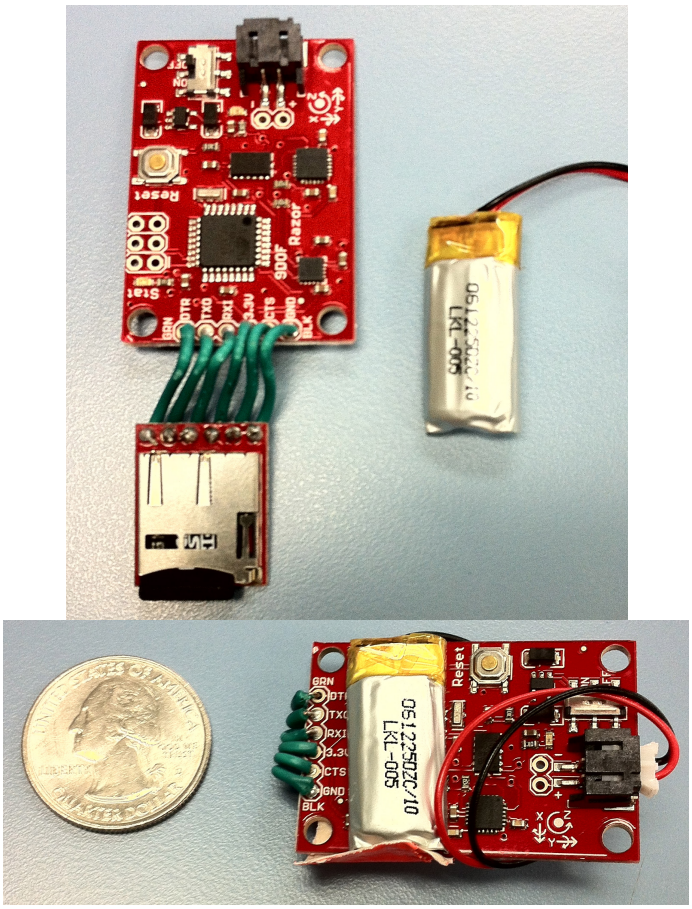


Figure 4.7: 9-DOF Inertial Measurement Unit, data-logging device, and li-ion battery;
Top: The IMU board contains the three sensors and a microprocessor to handle the data. Data is passed to the logging-unit where it is saved onto a microSD card. Power is supplied from a li-ion battery with 3.6V, 110-mAh output.
Bottom: Final instrument package before being attached to wing section.

Next, the samara wing form was investigated. With the payload mass already determined, the need for a light, but rigid wing structure was needed, and one that could handle the environmental conditions and easy to manufacture. A method using stereo-lithography with PLA thermoplastic material was utilized. A custom wing section could be modeled in any 3D CAD software. A model was printed from a bioplastic material (derived on renewable resources) using a 3D printer based on open source software. The 3D printer used had a 0.5 mm nozzle and could achieve a single layer thickness of 0.3 mm.

The second design prototype had two wing versions under investigation: (A) the

first was three layers thick planform with a 1.5 mm thick leading edge spar and a total mass of 6 grams; (B) a two layer thick planform with a grid-like pattern to remove additional mass, a 1.5 mm thick leading edge spar, and a total mass of 4 grams. The overall dimensions of the two wings were a wingspan of 13.5 cm and a max chord length of 6.1 cm. These dimensions were scaled up from the first iteration design using a constant aspect ratio to accommodate for the increase in payload mass. Both second iteration prototypes used a similar geometry as the first; however, the planform had an elliptical shape at the tip to reduce induced drag. The two versions of the samara wing planforms used for the second prototype are shown in Figure 4.8.

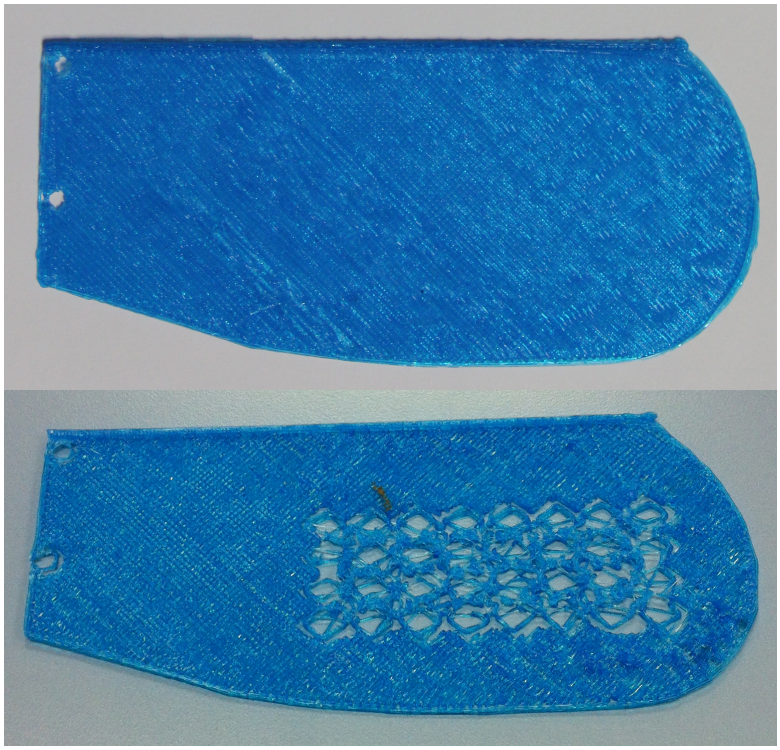

Figure 4.8: Top: Wing section type (a) 3 layers thick with 1.5mm leading edge spar and mounting holes
Bottom: Wing section type (b) 2 layers thick with 1.5mm leading edge spar and mounting holes

After calibrating the IMU to ensure proper functioning of the three sensors, the second samara prototype models, one shown in Figure 4.9, were test flown. In an effort to increase the descent distance for more data collection, the flight tests were conducted from the 6th floor balcony of the Engineering Research Building. The same IMU payload was used for each drop, and the data from the three sensors was recorded for each test. Multiple drops were conducted with each wind design.

Figure 4.9: Second samara prototype with wing type A described above

Figure 4.10 – 4.11 show sample raw output for the entire descent of two flight tests. Figure 4.10 shows the flight of the IMU board with wing type A, while Figure 4.11 shows the flight with wing type B.

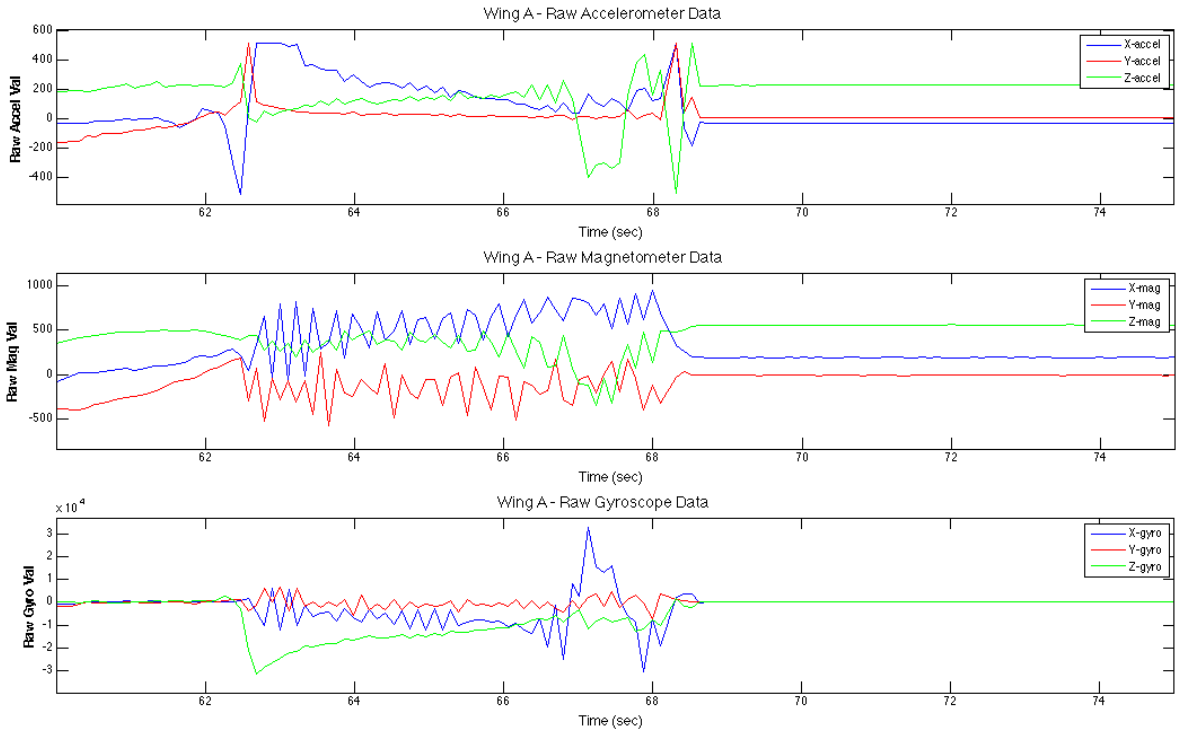


Figure 4.10: Raw Data recorded from a flight test with wing type A. The vehicle became unstable towards the end of the flight test

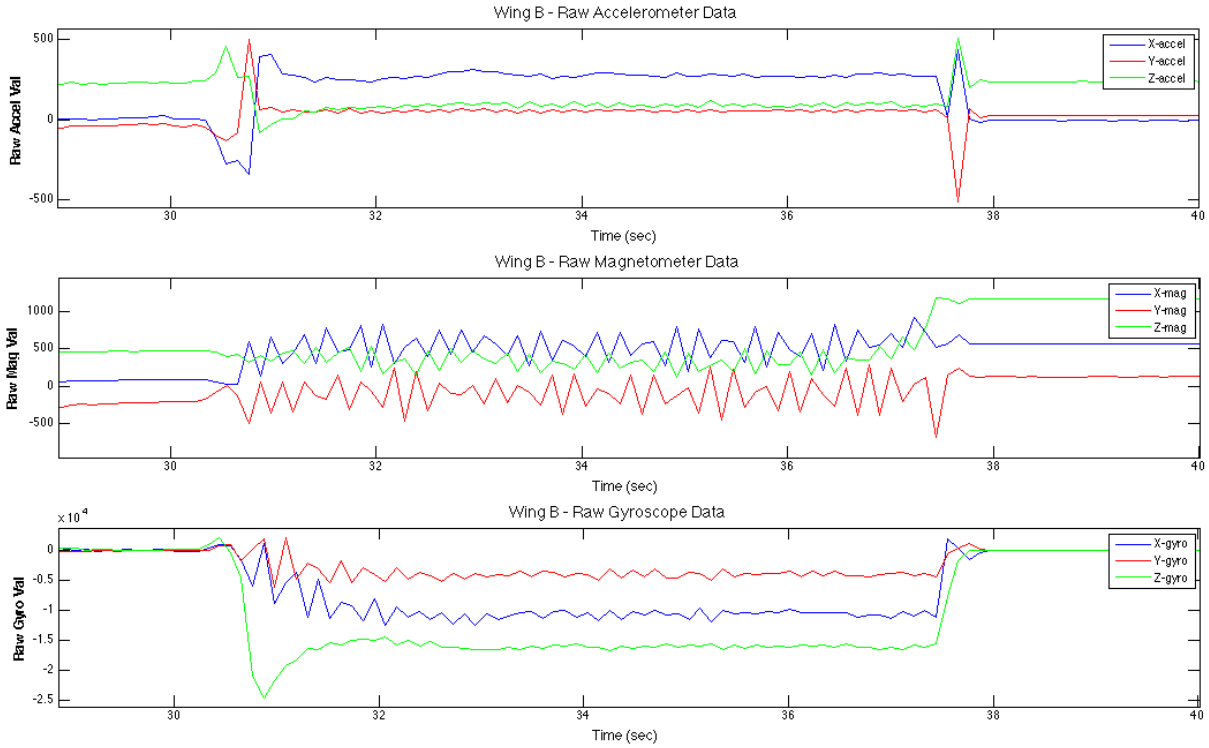


Figure 4.11: Raw Data recorded from a flight test with wing type B. The vehicle experienced stable flight throughout the entire flight test

The sensors provided raw recorded data in three axes. The values of particular interest that indicate a steady auto-rotating descent are the Z-axis accelerometer and Z-axis gyroscope readings, which indicate if the vehicle is in free fall and constant yaw-rotation respectively. The X-axis gyroscope reading indicates the coning angle. The X-axis accelerometer reading indicates whether the IMU is rotating, and the Y-axis accelerometer would indicate translation. The magnetometer readings indicate the direction the IMU board is pointing in three-dimensions with respect to the magnetic field strength it is measuring. A constant sinusoidal variation in the X and Y axes readings, with the Z-axis reading remains constant, would indicate a steady autorotation.

The flight tests lasted between 7.1-7.4 seconds. During the descent, the 3-layer prototype design experienced a slow descent rate, and towards the end of the descent, began to experience unsteady behavior and eventually led to unstable flight. This behavior can be seen in the data presented. The yaw-rotation rate was not constant (indicated by Z-axis of gyroscope), and the change in coning angle (X-axis gyroscope) began to fluctuate rapidly. The primary reason for this behavior was due to the weight of the wing section, and the CoM displacement from the root along the span of the wing. In order to achieve a stable flight, the CoM location must be closer to the payload mass, which requires a lighter wing structure.

The 4-gram, 2-layer prototype design experienced a smooth stable autorotation during the entire descent. The yaw-rotation and coning angle rate were constant throughout the flight. The Z-axis acceleration had a reading of 0 during the descent to indicate free fall. The X-axis acceleration was constant, while the Y-axis acceleration was 0, which indicates constant rotation but no translation. The X and Y magnetometer readings

experienced a constant, steady fluctuation while the Z-axis reading remained relatively constant, which also indicates a steady rotation.

The data obtained by the IMU can be further processed to give the Euler angle orientation of the board. A python script is being developed that reads the post-processed Euler angles from a given flight test, and graphically displays the orientation of the board during the flight, allowing for virtual playback of the flight test.

# CHAPTER 5

# DISCUSSIONS

The goal of this project was to create a distributed sensing device in the shape of a samara capable of performing an upper atmospheric weather mission. The effort began with high-level conceptual design and investigation into the mission architecture of a distributed radiosonde mission. This research prototyped a design that fit the requirements for such a mission. The investigation then progressed to the development of an analytical description of the flight characteristics of the samara-shaped sensing device. A time simulation was developed capable of testing various auto-rotating samara configurations in free flight. In parallel with the simulation, two iterations of free flight samara vehicles were designed and test flown. These efforts have led to several discoveries about the flight behavior of a samara.

## 5.1 Research Discoveries

*The use of a leading edge spar significantly increased the performance of the samara prototypes during flight tests.* This is due to the location of the chordwise CoM, which is discussed further below. The leading edge spar can also serve as a dual function for the communications subsystem in future iterations. The mission architecture discussed in Chapter 2 implemented a communications system capable of transmitting the collected data to a ground station. The CC430 is capable of handling the data and utilizing the built-in software radio to transmit the signal. The microprocessor still needs an external antenna to transmit the analog signal. A thin wire antenna can be incorporated into the vehicle design by placing it along the leading edge of the samara wing. This shifts the CoM position towards the leading edge in the chordwise direction as well as meets the requirement for

an active antenna for communication.

The chordwise CoM location plays an important role in the samara's flight characteristics. Norberg presented a study where the chordwise center of pressure (CP) location could be varied to provide pitch stabilization. The CP location is a function of angle of attack. When a disturbance causes a deviation from the equilibrium angle of attack, a restoring moment is generated as a result of the offset of the CP location. Figure 5.1 illustrates the relationship between the forces acting along the chord of a samara blade.

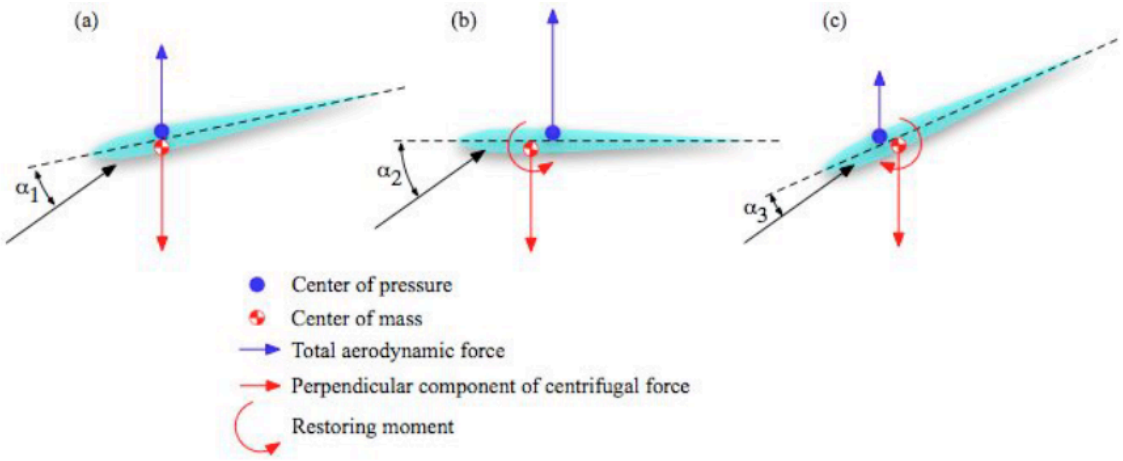


Figure 5.1: Samara pitch stabilization characteristics [22]

Depending on the airfoil being used, the chordwise location of the CP will vary with angle of attack. For this research, a flat plate was used with data provided by the NACA TN 3221 Technical Report. The CP variation data is presented in Figure 5.2:

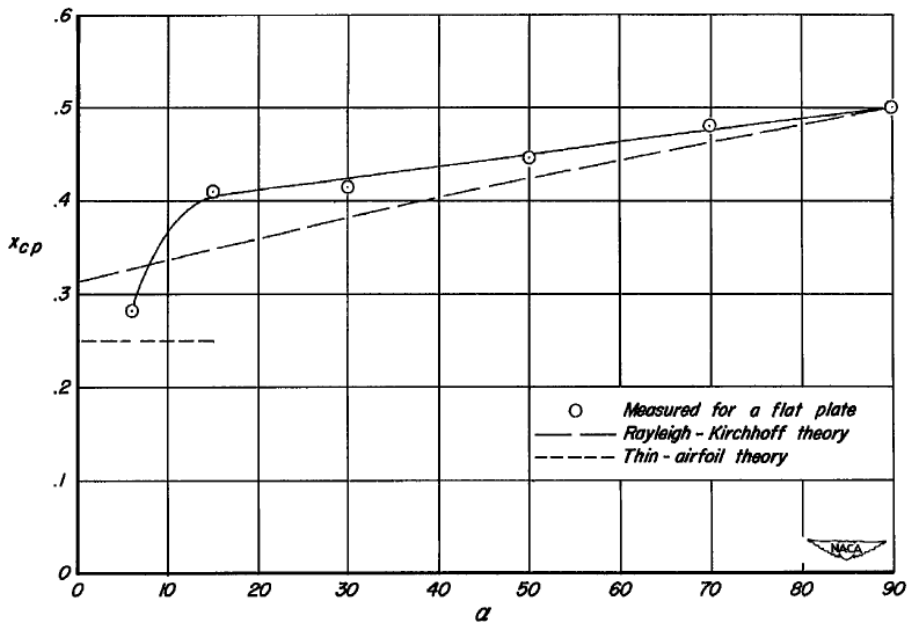


Figure 5.2 Center of pressure location (along the chord) as a function of angle of attack (deg) [24]

From the figure, it can be seen that as the angle of attack increases, the chordwise CP location approaches mid-chord. If the CoM location is behind of the CP location, a reduction in the angle of attack from the equilibrium position occurs and a restoring moment is generated to counter the unbalance. Similarly, if the CoM is ahead of the CP, an increase in angle of attack will also be countered by a restoring moment. A CoM location outside the minimum or maximum CP location would cause instability. Norberg presented that the best stability characteristics could be achieved with a CoM placement between the 27%-35% chord points [18].

The vertical axis also had an effect on pitch stability. A CoM location below the vehicle's CP location along the Z-axis results an a restoring moment in addition to the restoring moment generated by the variation in chordwise CP location. During flight tests, the direction of stable auto rotating flight generally coincided with a vehicle orientation

where the vertical CoM location was below the vehicle. However, it was concluded that the magnitude of the restoring moment created by this vertical offset was significantly smaller than the chordwise CP variation. Also, because the ideal design could be a system on a PCB, The overall thickness, and vertical mass displacement, would be very small values.

Norberg also reported through his research that the spanwise location of the CoM must lie between 0%-30% of the span length of the vehicle [18]. An ideal design would have a minimal descent rate, which serves as a performance feature as well as a stability feature. An important parameter that defines steady state autorotation is the coning angle. If the coning angle becomes too large, the helical tip path becomes stretched out which increases sideslip velocities that produce instability. If the CoM location is near the root, the center of rotation also moves towards the root, which increases the area swept by the wing. The increase in swept area minimizes the disc loading over the span, which minimizes the descent rate and coning angle during a samara flight.

## 5.2 Summary

Analytical and experimental studies were conducted to investigate the feasibility of creating a distributed sensing system with samara shaped sensing devices capable of operating in a wide bandwidth of altitudes. The primary goal was to create a sensing device capable of self-stabilization along with a minimal descent rate during its flight. To achieve this goal, the following steps were taken:

- Conceptual Design
- Investigation of science requirements for an upper atmosphere mission
- Conceptual mission design for an upper atmosphere mission
- Development of a 6 degree-of-freedom analytical model describing the steady state

auto-rotating descent of a samara

- Development of a time simulation to numerically solve the analytical model
- Design of prototype samara models
- Field experiments to validate the simulation
- Flight test of IMU sensing samara

The conceptual design resulted in several design parameters being chosen to define the solution space for a candidate vehicle for a distributed space mission. A mission design for observing the upper atmosphere was developed. This reference mission served as a test-bed validation of the research being conducted. An investigation into the science requirements for an upper atmosphere mission led to the selection of an instrument suite. This science payload had a total mass of 7 grams and the entire system, along with other subsystems required for operation could be incorporated onto a single PCB. A vehicle geometry based on a shape occurring in nature, the samara, was chosen for this reference mission because of its ability to maximize exposure time to the observation environment by minimizing descent rate.

Simulation and flight-testing results were required to investigate the flight behavior of the chosen vehicle geometry, the single wing samara. Insight into how this geometry creates a stable auto-rotating descent was needed in order to design a prototype vehicle. The simulation predicted descent and autorotation rates approximately 12.5% of experimentally observed performance. Incorporation of an inertial measurement unit allowed for real-time measurement of flight characteristics during flight tests, including accelerations, spin-rates, and heading.

A commercial 3D printer was utilized to create custom wing planforms. Different

wing planforms with varying design parameters could be designed and flight-tested to obtain experimental results. Based on the amount of material needed to create a samara wing section, this commercial printer proved a cost effective way to create multiple planforms. Each wing planform required $0.15 of material. The commercial printer produced wing sections with a high level of precision. These wing sections also survived multiple flight tests from a very high initial altitude.

# CHAPTER 6

# CONCLUSIONS AND FUTURE WORK

The goal of this research was the design and development of a self-stabilizing re-entry vehicle that closely resembles naturally occurring samaras in nature. It was hypothesized that a femto-satellite vehicle with a shape of a samara could self stabilize and passively generate lift, as well as transmit a signal during its descent through the atmosphere. An analytic simulation predicted the flight behavior of the samara. Then several prototype designs were test flown and their flights compared with the analytical results. This research concluded that it is feasible to design a samara device of this form factor that can successfully accomplish distributed space missions.

## 6.1 Future Work

It was hypothesized that flow separation caused by the leading edge spar on the leading edge of the flat plate cause flow separation, which induced pitch stability during autorotating flight. Further investigation into this stability behavior can be conducted.

Eagle CAD was used to design a notional PCB containing the science payload and data handling/communication capabilities detailed in Chapter 2. Figure 5.3.1 shows a potential configuration layout of a PCB capable of measuring weather parameters. The board does not show a power supply; however, a small lithium-ion battery identical to the one used with the IMU board prototype can be utilized with this hypothetical board.

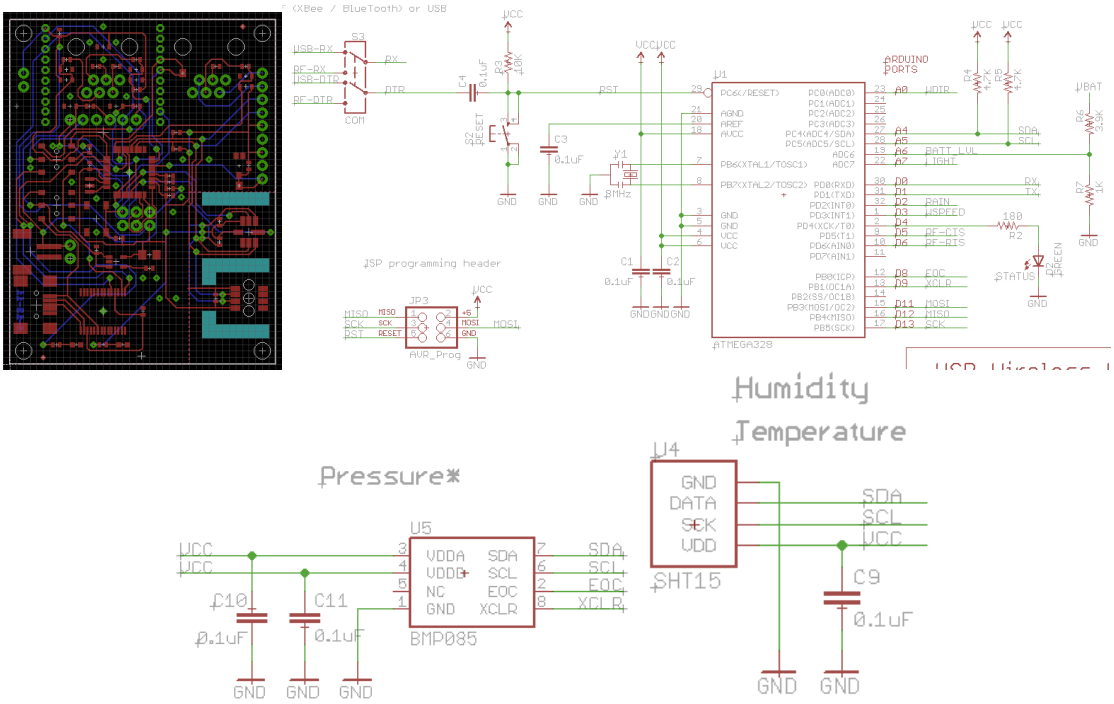


Figure 6.1 Board and schematic design with weather sensors; Dimensions: 6.1 cm x 5 cm x 1 cm

Integration of the communication is another goal to allow for real-time transmission of measured data from the sensing device to the ground station. A parent deployment device is also being investigated. This device should be capable of releasing the distributed sensing system into the target environment. With the successful integration of the above-mentioned goals, a distributed radiosonde mission using a weather balloon as the launch vehicle can be achieved.

REFERENCES


1. Cook, Ben, et al. “SoC Issues for RF Smart Dust”. Proceedings of the IEEE. Vol. 94, No. 6, June 2006. 1177-1196.

2. Burns, R.D., et al. “Radiation Forces on Small Particles in the Solar System”. Icarus Journal. 40. 1979. 1-48.

3. Shaw, G. B., Miller, D. W., and Hastings, D. E., **“**Generalized Characteristics of Communication, Sensing, and Navigation Satellite Systems,**”** Journal of Spacecraft and Rockets, Vol. 37, No. 6, 2000, pp. 801**–**811.

4. Krause, L. Habash, et al. “Microsatellite missions to conduct midlatitude studies of equatorial ionospheric plasma bubbles”. Advances in Space Research. 36. 2005. 2474–2479

5. Mumma, Michael J. et al. “Strong Release of Methane on Mars in Northern Summer 2003”. Science Magazine, Vol. 323, No. 5917, pp. 1041-1045.

6. Barnhart, David, et al. “Satellite Miniaturization Techniques for Space Sensor Networks”. JOURNAL OF SPACECRAFT AND ROCKETS. Vol. 46, No. 2. March–April 2009. 469-472.

7. Barnhart, David, et al. “A LOW-COST FEMTOSATELLITE TO ENABLE DISTRIBUTED SPACE MISSIONS”. United States Air Force. IAC-06-B5.6.06. 1-15.

8. Barnhart, David, et al. “Very-Small-Satellite Design for Distributed Space Missions”. JOURNAL OF SPACECRAFT AND ROCKETS. Vol. 44, No. 6. November–December 2007. 1294-1306.

9. Atchison, Justin and Mason A. Peck. “Length Scaling in Spacecraft Dynamics”. Journal of Guidance, Control, and Dynamics. Vol. 34, No. 1. January–February 2011. 231-246.

10. Whipple, Fred. “The Theory of Micro-Meteorites: Part 2”. Proceedings of the National Academy of Sciences. Vol 37. 1951. 19-30.

11. Whipple, Fred. “The Theory of Micro-Meteorites: Part 1”. Proceedings of the National Academy of Sciences. Vol. 36. 1950. 687-695.

12. Atchinson, Justin and Mason Peck. “A passive, sun-pointing, millimeter-scale solar sail”. Acta Astronautica. Vol. 67. 2010. 108-121.

13. Atchinson, Justin. “Microscale Atmospheric Re-Entry Sensors”. Cornell University, Space Systems Design Studio. June 14-18 2010.

14. Green, Douglas. “The Terminal Velocity and Dispersal of Spinning Samaras”. American Journal of Botany. Vol. 67. No. 8. September 1980. 1218-1224.
15. Burrows, F.M. “Wind-Borne Seed and Fruit Movement”. New Phytol. 1975. 405-418.

16. Peter Crimi. “Analytic Modelling of a Samara-Wing Decelerator”. American Institute of Aeronautics and Astronautics. 86-2439. 1986.

17. Peter Crimi. “Finite element analysis of a samara-wing decelerator”. Journal of Aircraft. Vol. 33 No. 4. 1996. 793-802.

18. Norberg, R. Ake. “Autorotation, Self-Stability, and Structure of Single-Wing Fruits and Seeds (Samaras) with Comparative Remarks on Animal Flight”. University of Goteborg. 2 April 1973. 561-595.

19. Seter, D. and A. Rosen. “Study of the Vertical Autorotation of a Single-Winged Samara”. Biological Review of the Cambridge Philosophical Society. Vol. 67 Issue: 2. May 1992. 175-197

20. Seter, D. and A. Rosen. “Vertical Autorotation of Single-Winged Samara”. Journal of Applied Mechanics. Vol. 58. December 1991. 1064-1071.

21. Gessow, Alfred and Gary C. Myers Jr. Aerodynamics of the Helicopter. College Park Press. 1999

22. Kellas, Andreas. “The Guided Samara: Design and Development of a Controllable Single-Bladed Autorotating Vehicle”. Massachusetts Institute of Technology. September 2007.

23. Morton, H. S. Jr. “A Formulation of Rigid-Body Rotational Dynamics Based on Generalized Angular Momentum Variables Corresponding to Euler Parameters”. American Institute of Aeronautics and Astronautics. 84-2023. 1984

24. Wick, Bradford. “Study of the Subsonic Forces and Moments on an Inclined Plate of Infinite Span. National Advisory Committee for Aeronautics. June 1954.

## BIOGRAPHICAL INFORMATION

Amit Lalloobhai graduated from the Georgia Institute of Technology in 2010 with a Bachelor of Science in Aerospace Engineering. During his time there, Amit performed wind tunnel experimentation research under Mark Costello, and competed in an AIAA undergraduate space design competition.

Prior to joining the University of Texas at Arlington, Amit received a one-year contract position at NASA Ames Research Center, where he worked on software research and development as part of the Next Generation Air Traffic Management System.

At the University of Texas at Arlington, Amit worked under Ben Harris in the Satellite Technology Laboratory in pursuit of a Master of Science in Aerospace Engineering, which he will be earning in May 2013. This research focused on the design and development of the femto-satellite concept.